RESTRICTED INVESTIGATION REPORT 1745R

CSIRO

INSTITUTE OF MINERALS, ENERGY AND CONSTRUCTION

DIVISION OF EXPLORATION GEOSCIENCE

MAGNETIC PROPERTIES AND MAGNETIC SIGNATURES OF THE TROUGH TANK AND STARRA COPPER-GOLD DEPOSITS, EASTERN MOUNT ISA BLOCK

(AMIRA PROJECT 78/P96B: APPLICATIONS OF ROCK MAGNETISM)

D.A. Clark

P.O. Box 136
North Ryde, NSW
Australia 2113

JULY, 1988

CSIRO
AUSTRALIA

Division of Exploration Geoscience
Delhi Road, North Ryde, NSW Postal Address: PO Box 136, North Ryde NSW 2113
Telephone (02) 887 8666. Telex AA25817 Fax (02) 887 8909

Chief: Dr B.J.J. Embleton

POLICY ON RESTRICTED INVESTIGATION REPORTS

Restricted Investigation Reports issued by this Division deal with projects where CSIRO has been granted privileged access to research material. In return for this access, they provide recipients with an opportunity to take advantage of results obtained on their samples or problems. Initially, circulation of Restricted Investigation Reports is strictly controlled, and we treat them as confidential documents at this stage. They should not be quoted publicly, but may be referred to as a "personal communication" from the author(s) if my approval is sought and given beforehand.

The results embodied in a Restricted Investigation Report may eventually form part of a more widely circulated CSIRO publication. Agreements with sponsors or companies generally specify that drafts will be first submitted for their approval, to ensure that proprietary information of a confidential nature is not inadvertently included.

After a certain period of time, the confidentiality of particular Restricted Investigation Reports will no longer be an important issue. It may then be appropriate for CSIRO to announce the titles of such reports, and to allow inspection and copying by other persons. This procedure would disseminate information about CSIRO research more widely to Industry. However, it will not be applicable to all Restricted Investigation Reports. Proprietary interests of various kinds may require an extended period of confidentiality. Premature release of Restricted Investigation Reports arising from continuing collaborative projects (especially AMIRA projects) may also be undesirable, and a separate policy exists in such cases.

You are invited to express an opinion about the security status of the enclosed Restricted Investigation Report. Unless I hear to the contrary, I will assume that in eighteen months time I have your permission to place this Restricted Investigation Report on open file, when it will be generally available to interested persons for reading, making notes, or photocopying, as desired.

B.J.J. Embleton
CHIEF OF DIVISION

Floreat Park
Location: Underwood Avenue, Floreat Park
Postal Address: CSIRO Private Bag, PO Wembley WA 6014
Telephone: (09) 387 4233
Telex: AA92178
Fax: (09) 387 6046

Lindfield
Location: Bradfield Road, Lindfield
Postal Address: PO Box 218, Lindfield NSW 2070
Telephone: (02) 467 6733
Telex: AA26296
Fax: (02) 467 1902

DISTRIBUTION LIST

	Copy No.
AMIRA	1-22
Cyprus Minerals Australia Company	23
CSIRO Division of Exploration Geoscience	
D.A. Clark	24
P.W. Schmidt	25
B.J.J. Embleton	26
A.A. Green	27
CSIRO IMEC Records	28

This is copy number 25 of 28.

TABLE OF CONTENTS

LIST OF FIGURES

LIST OF TABLES

ABSTRACT

Mineralised Au-Cu bearing quartz-magnetites (bifs) from the Starra and Trough Tank deposits of the Eastern Mt Isa Inlier are intensely magnetised and give rise to large magnetic anomalies, which significantly perturb the ambient geomagnetic field. The mean susceptibility of the Starra samples is 1.7 G/Oe. The mean susceptibility of the Trough Tank ironstone samples is 0.58 G/Oe, whereas the susceptibility estimated from the anomaly, constrained by the drilling information, is 0.47 G/Oe. Within bodies of such high susceptibility the induced magnetisation is attenuated and deflected away from the regional geomagnetic field direction by self-demagnetisation. Remanence makes only a minor contribution to the total magnetisation of these ironstones. The estimated Koenigsberger ratio is ~0.2. The remanence is predominantly directed steeply upwards and appears to be ancient.

Failure to incorporate the effects of self-demagnetisation into interpretation of magnetic anomalies arising from such bodies can lead to serious errors, particularly in interpreted dip. The induced magnetisation of the Trough Tank ironstones is deflected towards the plane of the sheet-like units by ~50°, leading to a comparable error in interpreted dip if self-demagnetisation is neglected. Failure to take into account deflection of the local geomagnetic field by the intense anomaly contributes an additional error of about 5° to the interpreted dip. These effects account for the original mis-targetting of drill holes at Trough Tank.

The general theory of self-demagnetisation and modelling of large amplitude anomalies is presented in this report. It is recommended that existing software for the calculation of total field magnetic anomalies be modified, in a straightforward manner, so that the calculated anomaly corresponds to what is actually measured by total field magnetometers. Software for processing magnetic anomaly maps, including upward/downward continuation, reduction to the pole and derivative calculations may also have to be modified to correct for departures of the measured field from the assumed potential field behaviour.

1. INTRODUCTION

This investigation is the final case study of the AMIRA project 78/P96B (Applications of Rock Magnetism). The Starra and Trough Tank deposits were chosen for study because they constitute an interesting, newly recognised, style of gold-copper mineralisation with strong magnetic signatures and because of the interpretational problems encountered during modelling. One aim of the study was to characterise the magnetic properties of this type of orebody, in order to assist exploration for similar deposits by predicting magnetic signatures which would be associated with such orebodies under various conditions (e.g. detectability of ironstone bodies within magnetic or non-magnetic host rocks as a function of thickness, strike extent and depth). A further aim was to assess the effects of remanence, self-demagnetisation, anisotropy, and the perturbation of the local geomagnetic field direction on the form of anomalies produced by these ironstone bodies, in order to develop guidelines for quantitative modelling of the magnetic signatures and thereby improve drill targetting.

An oriented block sample of oxidised bif (quartz-haematite) from the Starra decline, along with six partially oriented drill core samples of quartz-magnetite from the Starra deposit, were supplied by the Cyprus Minerals Australia Company. Details of the samples are given in Table 1. CSR Ltd supplied 22 drill core samples from the Trough Tank prospect (18 ironstone and 3 country rock samples), details of which are listed in Table 2, as well as ground magnetic contours and profiles over the main Trough Tank anomaly.

Several specimens (nominally 2.5 cm diameter by 2.2 cm height) were cut from each sample to provide duplicate analyses and to supply material for a variety of palaeomagnetic cleaning techniques. The bulk susceptibilities of the specimens were measured on the CSIRO balanced transformer susceptibility bridge, described by Ridley and Brown (1980). Magnetic remanence of the ironstone specimens was measured on a Digico fluxgate spinner magnetometer and remanence of weakly magnetised host rock specimens was measure using a CTF cryogenic magnetometer. A Digico anisotropy delineator was used for determination of magnetic fabric. The CSIRO non-magnetic furnace was used for step-wise thermal demagnetisation, whilst a Schonstedt GSD-1 demagnetiser was used for alternating field (AF) demagnetisation.

The sample mean remanences and susceptibility ellipsoids were calculated from the measured properties of the constituent specimens by vectorial and tensorial addition respectively. NRM directions and susceptibility axes are plotted on equal angle (Wulff net) and equal area (Schmidt net) stereograms respectively. Palaeomagnetic demagnetisation data are presented using orthogonal projections (Zijderveld plots). These methods of presentation have been described by Schmidt and Clark (1985).

2. GEOLOGY OF THE STARRA AND TROUGH TANK DEPOSITS

The Starra Au-Cu mine lies 150 km SE of Mt Isa, with the Trough Tank deposit a further 40 km to the south (see Fig.1). The deposits are hosted by rocks of the Middle Proterozoic Mary Kathleen Group and represent a newly recognised style of mineralisation. The mineralisation is closely associated with quartz-magnetite-haematite "ironstones" and has been variously interpreted as stratiform, bif-hosted, mineralisation analogous to volcanogenic massive sulphide deposits (Davidson et al., 1988) or as structurally controlled, syndeformational, metamorphic mineralisation (Laing et al., 1988).

The regional geological setting of the Starra and Trough Tank deposits has been described recently by Blake et al. (1983, 1984) and Blake (1987). References to earlier studies may be found in these publications. The Starra and Trough Tank deposits lie within the Mary Kathleen zone of the Eastern Fold Belt, which consists predominantly of Proterozoic cover sequence 2 and granite of the Mt Isa Inlier (Blake, 1987).

The geology of the Starra area has been described by Morrison(1986), Davidson (1987) and Davidson et al. (1988). Starra occurs near the base of the Staveley Formation, which consists mainly of well-bedded to locally brecciated sandy, silty and clayey sedimentary rocks. Apparently conformable banded quartz-haematite-magnetite rocks within the Staveley Formation form prominent ridges which extend for many kilometres. In the vicinity of Starra, two north-south trending ironstone ridges, about one kilometre apart (the "Eastern" and "Western" Ironstones), outcrop for 15 km. The deformed, conformable, steeply dipping ironstones are hosted by variably feldspathic, micaceous and calcareous iron oxide bearing schists and calc-silicates. The pre- or syn-tectonic Gin Creek Granite outcrops 500 m west of the Western Ironstones and the post-tectonic Mt Dore Granite outcrops 500 m east of the Eastern Ironstones.

The Eastern and Western Ironstones are linked at one point by a fold closure known as the Hinge Zone. The Western Ironstone is magnetite-rich, and hence is strongly magnetic, and contains several mineralised zones. On the other hand, the Eastern Ironstone is haematite-rich, weakly magnetic and generally unmineralised. The Staveley Formation conformably to unconformably overlies the quartzites and schists of the Kuridala Formation to the east and possibly equivalent micaceous schists of the Answer Slate to the west. Significant mineralisation is confined to quartz-magnetite rich ironstones, except for Area 244, where feldspathic and chloritic, magnetite-bearing schistose breccia is mineralised. Footwall chloritic and feldspathic magnetite schists are weakly mineralised, whereas the hangingwall calcareous rocks are generally unmineralised. Current reserves are estimated at 4.5 million tonnes of 4.5 g/t Au and 2% Cu (Mock et al., 1988).

The Starra area has experienced a complex structural and

magmatic history, which obscures genetic relationships. Davidson et al. (1988) recognise four deformational episodes:

D_1 - regional thrusting, with development of a 500 m wide mylonite extending west into the Gin Creek Granite, which is surrounded by a high grade contact aureole,

D_2 - regional, shallowly plunging, north-trending isoclinal folding, coinciding with peak metamorphism, predated by widespread amphibolite intrusion,

D_3 - medium scale, sinistral, steeply plunging folds generated by strike-slip movement on a reactivated D1 mylonite surface,

D_4 - east to west thrusting along the Mt Dore Fault and further activation of the D1 surface, apparently synchronous with regional intrusion of the Williams Batholith at 1500 Ma. This event is responsible for the structural control of several copper deposits in the Cloncurry District (e.g. Mt Dore).

The geophysics of the Starra deposit has been discussed by Collins (1987). The mineralised, magnetic Western Ironstones are clearly defined by detailed aeromagnetics, producing anomalies of several tens of nT, whereas the Eastern Ironstones produce negligible response. Ground magnetic anomalies over the known mineralised zone are dominated by the effects of the magnetite-bearing footwall schists which produce high amplitude, relatively broad anomalies. Filtering of the airborne and ground magnetic data has been able to separate 50 nT, short wavelength residual anomalies associated with ironstone from 5000 nT, long wavelength anomalies arising from the footwall schists. Although the mineralised horizon is associated with a well-defined magnetic anomaly, within this horizon there appears to be no general relationship between grade and magnetic properties.

The Trough Tank prospect was originally located by aeromagnetics. The ironstone mineralisation lies beneath 30-40 m of Mesozoic cover rocks of the Eromanga Basin, with no surface geological or geochemical expression, and therefore represents a truly "blind" geophysical target. The geology and geochemistry of the Trough Tank prospect have been discussed by Davidson (1987) and Davidson et al. (1988). The host rocks are tentatively correlated with the uppermost Kuridala Formation and the style of mineralisation is thought to represent a less deformed equivalent of the Starra deposit. The mineralisation is entirely confined to thick well-banded quartz-magnetite-haematite rocks within middle amphibolite grade metamorphic host rocks. The rocks were folded during D2, but D1, D3 and D4 did not significantly affect the area and there are no nearby granitic intrusions. The structural and stratigraphic relationships are therefore more straightforward at Trough Tank than at Starra.

The geophysics of the Trough Tank Prospect has been discussed by Gidley (1988). A huge ground magnetic anomaly (16,000 nT maximum amplitude) with a NW-SE strike is associated

with the ironstones. There is virtually no high frequency noise on the magnetic profiles due to the thickness of non-magnetic overburden. Initial interpretation of the magnetic anomaly assumed magnetisation by induction, parallel to the present field direction, and indicated a SW dip. The first two diamond drill holes failed to intersect the source of the anomaly. After further drilling had intersected thick highly magnetic ironstones it was realised that the interpreted dip had been seriously in error and that the units in fact dip 45-50° NE.

Erroneous dips interpreted from magnetic anomalies usually reflect the presence of significant remanent magnetisation with a direction oblique to the present field. Thus remanence was suspected to be causing the dip discrepancy, but measurements of the susceptibilities and natural remanent magnetisations (NRMs) of a number of ironstone samples by Prof. D.W. Emerson of the University of Sydney showed that remanence made only a minor contribution to the total magnetisation and could not account for the discrepancy. The error in the interpreted dip is attributable to two main effects:

(i) self demagnetisation, due to the very high susceptibility,

(ii) perturbation of the regional geomagnetic field by the very large local anomaly.

The theory of magnetic interpretation of intense anomalies arising from bodies of high susceptibility is discussed in section 4, and application of the theory and the magnetic property measurements to interpretation of the Trough Tank anomaly is treated in subsequent sections.

3. MAGNETIC PROPERTIES OF THE STARRA AND TROUGH TANK SAMPLES

The apparent susceptibilities and remanences of the strongly magnetic ironstone specimens are affected by self-demagnetisation and must therefore be corrected in order to yield the corresponding intrinsic properties. The relationship between the true susceptibility k and apparent susceptibility k′ is (Clark, 1979, and section 4):

$$k' = k/(1+Nk), \qquad (1)$$

where N is the demagnetising factor along the direction of measurement (assuming this corresponds to a symmetry axis of the specimen, so that the demagnetising field is collinear with the magnetisation).

This can be solved for true susceptibility, yielding:

$$k = k'/(1-Nk'). \qquad (2)$$

The corresponding relationships for true remanence, J, and apparent remanence, J′, are:

$$J' = J/(1+Nk), \quad (3)$$

$$J = J'(1+Nk). \quad (4)$$

The demagnetisation-corrected sample mean susceptibilities, NRMs and Koenigsberger ratios of the Starra and Trough Tank samples are given in Tables 3 and 4 respectively. The decline sample is the only one from either locality which was oriented in situ. All the drill core samples are only partially oriented: the top of the cores was marked and the attitude of the core axes was known from the drill hole surveys, but the samples were azimuthally unoriented, when supplied. Thus, although the remanence directions of specimens cut from each sample can be related to one another, and the angle between the remanence and the up-hole direction can be be defined, the relative orientations of remanence vectors from different samples cannot be uniquely determined, nor can their absolute orientations with respect to geographic co-ordinates. Orientations of remanence vectors and magnetic fabric axes can only be defined to lie somewhere on cones centred on the core axis. If a remanence vector or susceptibility axis is fortuitously aligned with the DDH axis, the absolute orientation is defined. In some cases the angle between the remanence and the DDH axis is small and the remanence direction is then quite well-defined.

An attempt was made to orient the samples azimuthally by using the magnetic fabric. The magnetic foliation (plane of relatively high susceptibility) is parallel to the banding in ironstone samples and to the schistosity in host rock samples. Assuming the holes were drilled normal to strike, and knowing the general dip of the schistosity and ironstone banding, at least approximately, it is possible to determine uniquely the azimuthal orientation by rotating (conceptually) the samples until the strike of the magnetic foliation coincides with the known strike of the banding and schistosity. Although the mean dip of the magnetic foliations, obtained using this method of orientation, corresponds reasonably well with the general dip of the structures, as estimated from the drill sections, there is considerable variability in dip, presumably reflecting the structural complexity of these deposits. Reasonably consistent remanence directions for different samples were obtained using this method, although for some samples there may be considerable error in azimuthal orientation.

The NRM directions of individual specimens from the unoxidised Starra ironstone samples and from the oxidised Starra decline sample are plotted in Fig.2 and Fig.3 respectively. NRMs of the quartz-magnetite rich specimens are generally directed steeply upwards, whereas the directions from the oxidised sample are scattered, although predominantly upward-pointing. The NRM directions for specimens from the Trough Tank samples are plotted in Fig.4. The directions are quite scattered, and appear to be

streaked between a steep up (normal polarity) direction and a steep down reversed direction, with upward pointing directions predominating.

The measured NRMs of coarse-grained magnetite bearing specimens is sometimes contaminated by palaeomagnetic noise acquired during drilling and slicing of the samples. This spurious remanence, when present, appears to be carried by the magnetite grains at the surface and is attributed to piezoremanence acquired when the grains were cut. Selected specimens were soaked in concentrated hydrochloric acid for 1-2 hours in order to dissolve the surface grains and the remanence was remeasured. Contamination of the NRMs by piezoremanence was found to be negligible. AF and thermal cleaning was also carried out on specimens from each sample, in order to resolve remanence components with different stabilities. Very soft remanence components with no consistency in direction from sample to sample represent palaeomagnetic noise picked up by exposure to magnetic fields during or after collection and are therefore not representative of the in situ magnetisation.

Palaeomagnetic cleaning showed that the measured NRMs are dominated by single components which are stable to 200 Oe, or higher, AF and to 570°C thermal demagnetisation. The AF cleaned (200 Oe) and thermally cleaned (550°C) remanence directions for the Starra quartz-magnetite rich specimens are plotted in Fig.5 and Fig.6 respectively. The cleaned directions are predominantly steep up. The AF cleaned (140 Oe) and thermally cleaned (550°C) directions for Trough Tank ironstone specimens are plotted in Fig.7 and Fig.8 respectively. The scatter of directions has been somewhat reduced by the cleaning and by the omission of the host rock specimens from these plots, and the pattern of roughly antiparallel normal and reversed components is clearer in these plots than in Fig.4. The overall stability of the NRMs to cleaning and the lack of clustering around the internal field direction (the present field direction deflected towards the plane of the bodies by self-demagnetisation) suggests that the NRMs are not viscous remanent magnetisations (VRMs) acquired recently, but are probably ancient.

Detailed examination of the palaeomagnetic cleaning data is best accomplished by using Zijderveld plots. Fig.9 provides an explanation of this method of presentation. Representative Zijderveld plots for AF and thermal demagnetisation of specimens from Starra and Trough Tank are shown in Fig.10 and Fig.11 respectively. Projections of remanence vector end points onto the horizontal plane are denoted by filled squares and projections onto the specified vertical plane are denoted by open squares. In most cases the NRMs of the specimens are dominated by a single remanence component, represented by long linear segments for corresponding points of both projections. In some cases these linear segments do not head directly for the origin, showing that there is a minor residual component of remanence, acquired at a different time, in these specimens. This residual component is usually not fully resolved by the demagnetisation. Some specimens

(e.g. STARRA 284B) appear to bear a soft component, which is removed during initial cleaning, and which may represent palaeomagnetic noise. The overall contribution of such components to the mean remanence vector calculated for all samples appears to be negligible, however.

The Trough Tank ironstone specimens exhibit similar behaviour to those from Starra, but the directions are generally more scattered. There is little evidence in the plots that the scatter is due to overprinting of a consistently oriented component by one or more components with distinct stability spectra. As discussed above, the orientation method is only approximate, but the scatter and the dual polarity cannot be explained by misorientation alone. The distribution of remanence directions most probably reflects prolonged acquisition of remanence, possibly by grain growth or recrystallisation during metamorphism. On the basis of the palaeomagnetic cleaning, the measured NRMs of the samples appear to correspond to essentially uncontaminated in situ magnetisations and can therefore be used to estimate the contribution of remanence to the magnetic anomalies, assuming the sampling of the ironstones is reasonably representative. Some of the scatter of directions probably reflects the inhomogeneous internal field within such highly magnetic bodies, reflecting heterogeneous distribution of magnetic material, irregular boundaries and the gross non-ellipsoidal geometry of the bodies. This effect means that strongly magnetic bodies are generally not very suitable for palaeomagnetic determination of ancient field directions and palaeopoles.

Although the oxidised ironstone sample from the Starra decline is quite magnetic by normal standards, it is much less magnetic than the unoxidised ironstone samples from deeper levels. The susceptibilities of the quartz-magnetite rich samples from the Starra deposit are exceptionally high, averaging 1.7 G/Oe. A susceptibility as high as this implies that self-demagnetisation has a pronounced effect on the direction and magnitude of induced and remanent magnetisation. Thus the form of the magnetic anomaly arising from the Starra ironstone should be influenced profoundly by self-demagnetisation. The Koenigsberger ratios of the Starra samples, particularly the samples with the highest susceptibilities, are generally less than unity, implying that induced magnetisation makes a greater contribution than remanence to the total magnetisation of these samples. Furthermore, because the NRM directions of the samples are somewhat variable, the vector mean NRM intensity for the deposit, based on these samples, is reduced with respect to the arithmetic mean of the sample NRM intensities. This accounts for the relatively low estimated Q value (0.21) for the combined quartz-magnetite samples. The mean susceptibility of the Trough Tank ironstone samples is lower than for Starra, but is still very high (0.48 G/Oe) and indicates the importance of self-demagnetisation for the form of the Trough Tank anomaly. The Koenigsberger ratio determined from the vector mean of the sample NRMs ($Q = 0.18$) is similar to the value for Starra.

Magnetic fabric, as defined by anisotropy of susceptibility, has been discussed by Clark and Embleton (1980), Clark (1988) and Clark et al. (1987). The principal susceptibility axes of specimens from the oriented oxidised ironstone sample from the Starra decline are plotted in Fig.12. This sample has a well-defined magnetic fabric with a shallow SSW-plunging magnetic lineation (maximum susceptibility axis) within a SSE-dipping magnetic foliation (plane of relatively high susceptibility, containing the maximum and intermediate susceptibility axes) normal to the minimum susceptibility axis (the magnetic foliation pole). The degree of anisotropy of this sample is not particularly large ($A = k_1/k_3 = 1.08$).

The magnetic fabric of specimens from the Starra quartz-magnetite rich ironstone samples is shown in Fig.13. The azimuthal orientation of these samples was determined by rotating the samples until the sample mean magnetic foliation poles were normal to the geological strike. It is not surprising, therefore, that the plotted minimum susceptibility axes have consistent WNW declinations. The declinations of k_3 axes are not all identical because of variability of magnetic fabric from specimen to specimen within samples. The good grouping of minimum axes in Fig.13 therefore indicates that the magnetic fabric within samples is quite consistent. The magnetic foliation coincides with the visible banding in these samples and the susceptibility anisotropy is therefore textural, arising from anisotropic self-demagnetisation of the high susceptibility magnetite-rich bands. Fig.13 indicates a subvertical NNE-striking magnetic foliation, subparallel to the lithological boundaries and the mesoscopic banding, containing a steeply plunging magnetic lineation, which may reflect the steeply plunging sinistral folds within the Western Ironstones and Hinge Zone. The anisotropy degree of these samples is typically about 10% ($A = 1.10$), which is not sufficient, in itself, to deflect induced magnetisation by more than a few degrees.

The magnetic fabric of the Trough Tank specimens is shown in Fig.14. The above comments about orientation and scatter of minimum axes also apply here. At Trough Tank the NW-striking magnetic foliation appears to be subvertical, i.e. steeper than the lithological contacts which dip about 50° NE. This may reflect F_3 flexures which are invoked to explain dip variations of banding within the ironstones (Davidson, 1987). In contrast to Starra there is no well-defined magnetic lineation at Trough Tank. The anisotropy degree of the Trough Tank samples is similar to that of the Starra samples (about 10%).

In summary, the very high susceptibilities of the ironstones confirm the controlling influence of self-demagnetisation on the magnetisation of the ironstone bodies, and hence on the form of the associated anomalies. Remanent magnetisation is of secondary importance, representing only about 20% of the induced magnetisation. The net remanence direction in both bodies is steep up and appears to be ancient.

4. PRINCIPLES OF INTERPRETATION OF INTENSE MAGNETIC ANOMALIES

4.1 Non-uniqueness in Magnetic Interpretation

Magnetic anomalies arise from subsurface distributions of magnetisation. The purpose of magnetic interpretation is to determine the geometry and magnetisation of the sources, on the basis of certain assumptions (without which the solution is non-unique). As an example, the source is often assumed to have a simple geometry, based on plausible geological models, and is assumed to be homogeneous. This approach is necessary because in practice very complex structure and small-scale heterogeneity cannot be resolved by magnetic data, and in any case interpretation of such features would, even in principle, be hopelessly ambiguous because many different source distributions could produce identical magnetic signatures. The magnetic method is useful because geological bodies, in many cases, can be represented reasonably well by simple geometries and are characterised by distinctive, macroscopically relatively uniform, physical properties. Definitive determination of the geometry of even simple subsurface bodies requires either extra information (from geology, drilling, other geophysical methods or magnetic property measurements) or additional a priori assumptions in order to constrain models and eliminate ambiguity.

4.2 Component and Total Field Magnetic Anomalies

Denote the regional unperturbed geomagnetic field vector by **F** and its magnitude by F. The magnitude and direction of **F** can be taken as constant over a local survey area. At any survey point, the local distribution of magnetisation gives rise to an anomalous magnetic field, **B**, which adds vectorially to the regional field to give a resultant field, $\mathbf{F'} = \mathbf{F} + \mathbf{B}$ (Fig.15). The regional field, the local anomalous field and the resultant field vectors have components with respect to geographic axes (+x = true north, +y = true east, +z = down):

$$\mathbf{F} = (F_x, F_y, F_z), \tag{3}$$

$$\mathbf{B} = (B_x, B_y, B_z), \tag{4}$$

$$\mathbf{F'} = (F'_x, F'_y, F'_z) = (F_x + B_x, F_y + B_y, F_z + B_z). \tag{5}$$

In the vicinity of magnetic bodies the resultant field varies both in magnitude and direction. "Total field" magnetometers, such as proton precession or optical pumping magnetometers, measure the magnitude of the resultant field, F', irrespective of its direction. The measured total field anomaly, denoted by B_m, is therefore the difference between the intensity of the local resultant field and the background level, i.e. the regional intensity. Thus

$$B_m = |\mathbf{F'}| - |\mathbf{F}| = F' - F. \tag{6}$$

In terms of components, eqn 6 may be written

$$B_m = [(F_x + B_x)^2 + (F_y + B_y)^2 + (F_z + B_z)^2]^{1/2} - F, \qquad (7)$$

where

$$F = [F_x^2 + F_y^2 + F_z^2]^{1/2}. \qquad (8)$$

The magnitudes of the resultant and unperturbed fields are related by

$$F'^2 = (\mathbf{F} + \mathbf{B}).(\mathbf{F} + \mathbf{B}) = F^2 + B^2 + 2\mathbf{F}.\mathbf{B}, \qquad (9)$$

$$\therefore B_T = (\mathbf{F}.\mathbf{B})/F = (F'^2 - F^2 - B^2)/2F, \qquad (10)$$

where B_T is the component of the anomalous field vector **B** projected onto the unperturbed field direction (see Fig.15).

Eqn (10) can be rewritten

$$B_T = [(F' - F)(2F + F' - F) - B^2]/2F,$$

$$\therefore B_T = (F' - F) - [B^2 - (F' - F)^2]/2F. \qquad (11)$$

Thus, from (6) and (11)

$$B_T = B_m - [B^2 - B_m^2]/2F. \qquad (12)$$

It can be seen from Fig.15 that $B_m^2 < B^2$. It follows from (12) that when the magnitude of the anomalous field is everywhere small compared to the regional field ($B \leq B_{max} << F$), the second term on the RHS of eqn (12) is negligible compared to the maximum anomaly amplitude. For example, if B_{max} is 500 nT (corresponding to B_m and B_T amplitudes of several hundred nT) and F is 50,000 nT, the error term is only ~2.5 nT. Therefore

$$B_T \simeq B_m \qquad (B_m << F). \qquad (13)$$

Equation (13) is exact only at points for which **B** and **F** are collinear, when $B_m = B_T = B$. The difference between B_m and B_T is therefore attributable to deflection of the geomagnetic field away from the undisturbed direction by the local anomalous field. The approximation of eqn (13) was introduced by Hughes and Pondrom (1947) and is valid to within 1% for anomalies less than 2% of the regional geomagnetic intensity (e.g. anomalies less than 1000 nT in a regional field of 50,000 nT). Since introduced, this approximation has been the basis of all subsequent magnetic modelling methods in the literature. The assumption that the anomalous field does not significantly perturb the direction of the regional field is deeply embedded in published algorithms for interpretation of magnetic surveys as well as processing methods based on potential field theory, such as upward and downward continuation, derivative calculations, reduction to the pole, pseudogravity, susceptibility mapping etc.

The error, E, in the approximation of eqn (13) is given by

$$E = B_m - B_T = [B^2 - B_m^2]/2F. \qquad (14)$$

Note that E is always positive, because $B > |B_m| > 0$. Thus at every point

$$B_m \geq B_T. \qquad (15)$$

For example, when the anomalous field vector is perpendicular to the regional field $B_T = 0$, by (10), but B_m is positive because **F'** is then the hypotenuse of the right angled triangle formed by **F**, **B** and **F'**, so that $F' > F$ (see Fig.15). For a given magnitude of anomalous field the maximum error occurs for $B_m = 0$, i.e.

$$E_{max} = B^2/2F. \qquad (16)$$

B_z is still occasionally measured, for example by vertical fluxgate magnetometers, and much vertical component data is available. As already mentioned, modern total field magnetometers determine B_m. Airborne fluxgate surveys continually re-orient the fluxgate to maintain parallelism with the resultant field by maximising the signal. Thus total field airborne fluxgate surveys also measure B_m. B_T is never measured in practice, but could be measured in principle by a single axis instrument, such as a fluxgate, maintaining a fixed orientation parallel to the regional field (by use of gyroscopes, for instance). Horizontal components are almost never measured now, but the obsolete horizontal balances in fact measured the changes in magnitude of the horizontal component of **B**, $(B_H)_m$, rather than the projection of **B** onto the regional magnetic meridian (Fig.15). The conventional approximation used in interpreting horizontal component data, $(B_H)_m = B_H$, is analogous to eqn (13).

4.3 Nature of the Potential Field Approximation for Total Field Anomalies

B_T is the component, parallel to the regional geomagnetic field, of the external magnetic field produced by a magnetisation distribution. Thus B_T is the directional derivative, along a fixed direction in space, of the magnetic scalar potential, V, arising from the subsurface sources, i.e.

$$B_T = dV/ds = \text{grad } V \cdot \mathbf{s},$$

where **s** is the unit vector parallel to **F**.

V obeys Laplace's equation everywhere:

$$\text{div grad } V \equiv 0,$$

$$\therefore \text{ div grad } (dV/ds) \equiv (d/ds)\,\text{div grad } V \equiv (d/ds)\,(0) \equiv 0.$$

Thus B_T also obeys Laplace's equation and is therefore a

potential field. The same argument applies to magnetic field components along any fixed direction, e.g. B_x, B_y, B_z, which are also potential fields, with many useful mathematical properties. In particular, values of any one component on a surface, such as the surface over which a magnetic survey was conducted, determine the values of all components (and hence the complete vector) throughout the source free region, at least in principle. This is the basis for upward and downward continuation of magnetic survey data. Continuation of potential fields is a simple linear filtering operation (convolution filtering in the space domain or multiplication of the spectrum by a transfer function in the frequency domain). Other useful operations which can be accomplished by linear filtering include: calculation of one component from another (e.g. B_z from B_T), calculation of vertical derivatives of field components, reduction to the pole, pseudogravity transformation, and apparent susceptibility mapping.

The approximation (13) was originally introduced to justify reduction of measured total field (B_m) data, from a then new generation of magnetometers, to produce B_z maps, which are more easily interpretable. Hughes and Pondrom (1947) pointed out the nature of the approximation and the possibility of corrections being required when the assumption of negligible deflection of the geomagnetic field by the anomalous field does not hold. However this caveat has been virtually ignored, and the assumption of the validity of eqn (13) has become entrenched in the literature.

Kontis and Young (1964) reported an airborne vector magnetometer survey over a seamount. The magnetic component data allowed a direct comparison of the calculated B_T anomaly with the scalar intensity anomaly B_m. In a regional field of 51,300 nT, a 4000 nT B_m anomaly along a E-W profile was associated with maximum inclination anomalies of -1^o to $+0.5^o$ and declination anomalies of -6^o to $+2^o$. Along a N-S profile the maximum declination anomaly was -2.5^o and the inclination anomaly was $\pm 2^o$. The corresponding error in eqn (13) was found to be up to 50 nT, or ~1% of the total anomaly amplitude. Although the error was small in this case, it can be seen from (16) that the relative error, E_{max}/B, is proportional to the anomaly amplitude. Thus for very strong anomalies the difference between B_m and B_T is not trivial. Table 5 gives maximum errors as a function of ambient field strength and anomaly magnitude.

Calculation of B_m for a magnetic model is in fact no more difficult than calculating B_T, so the historical tradition of published formulae and software for magnetic modelling, which all calculate B_T, is quite unnecessary. Existing software can be simply modified to calculate theoretical B_m anomalies for models, which correspond to what is actually measured. The anomaly components B_x, B_y, B_z are always calculated as intermediate results in order to obtain B_T from the relationship

$$B_T = (\mathbf{B}.\mathbf{F})/F = (B_xF_x + B_yF_y + B_zF_z)/F. \qquad (17)$$

Thus B_m can be calculated from B_x, B_y, B_z using eqn (7). When the anomaly amplitude is a substantial fraction of the geomagnetic field, as at Trough Tank, the difference is large.

A number of tenets of magnetic modelling have to be changed, once it is realised that the measured anomaly is not a component along a fixed direction and that it is not strictly a potential field. For example, given a fixed model geometry and magnetisation direction, the amplitude of component anomalies (including B_T) is proportional to the magnetisation intensity and the anomaly shape is independent of intensity. This does not apply to intense B_m anomalies, because the distortion of the ambient field increasingly affects the anomaly shape as the anomaly amplitude increases. B_T and other component anomalies arising from multiple sources obey linear superposition, i.e. the anomaly due to two or more bodies with specified magnetisations is equal to the sum of the anomalies which would arise from each body in isolation. This does not apply to B_m anomalies, because of the non-linear relationship, eqn (10), between B_m and the component anomalies. It is therefore essential to calculate B_m from the components B_x, B_y, B_z for the multiple body, rather than summing B_m anomalies of individual bodies.

The applicability of the various filtering operations, such as continuation, to measured total field surveys is a more complicated issue. For example upward continuation of the measured Trough Tank ground magnetics would significantly distort the predicted field at airborne survey height, because of the substantial difference between B_m and B_T at ground level compared to the much smaller discrepancy at height. Two methods for correct continuation, reduction to the pole etc. seem applicable:

(i) An iterative method, suggested by Hughes and Pondrom (1947), which entails calculation of component anomalies by standard methods of potential theory, assuming $B_m = B_T$. These estimated components are then used to calculate new estimates of B_m and B_T, using (7) and (17). The process is repeated, using the updated estimate of B_T, until the discrepancy between the measured and calculated B_m is negligible. The derived B_T can then be filtered in the usual manner and, finally, a filtered version of B_m can be calculated from the resultant filtered values for the component anomalies.

(ii) Inversion of the measured total field data, using correctly formulated forward calculation of B_m, to obtain an equivalent source distribution, which is then used for direct calculation of component anomalies or B_m at different levels, reduced to the pole etc.

These methods assume that determination of the magnetic potential and field components from B_m is a well-posed problem, with a unique solution. B_m is certainly determined everywhere above all sources by complete knowledge of any one component over a surface in the source free region, since all other components

are determinable (by application of potential theory) and B_m is related to the components by eqn (7). The truth of the converse is, however, unknown. Backus (1968) has investigated the general non-linear boundary problem of determining a potential field throughout a source-free region when the magnitude, but not the direction, of the gradient of the potential is known on the boundary of the region. He obtained some partial results which suggest that the potential U may be determined throughout the exterior of a bounded surface, that encloses all sources, by the magnitude of the corresponding field, |grad U|, on the boundary. It is intuitively plausible that B_m measured over a surface determines the magnetic potential, and hence the field components, above that surface. Backus (1968) proved theorems which establish, for example, that knowledge of F′ (which is equivalent to knowledge of B_m) throughout the exterior of a volume enclosing the sources is sufficient to determine the exterior potential everywhere. Furthermore, if the magnetisation distribution represents multipole sources of finite order, B_m is determined everwhere above a survey surface by its values on the surface. The contrasting mathematical properties of B_m and B_T are summarised in Table 6.

4.4 The Demagnetisation Tensor, Demagnetising Factors and the Self-demagnetising Field

As well as ignoring the difference between B_m and B_T, many modelling programs ignore the effects of self-demagnetisation on the resultant magnetisation of magnetic bodies. This omission is unimportant if the body has low-to-moderate susceptibility ($k < 0.01$ G/Oe, say). For bodies of susceptibility greater than about 0.1 G/Oe, self-demagnetisation can significantly decrease the magnetisation and deflect it towards the long axis, if the body is elongated, or towards the plane of the body, for sheet-like geometries. As will be shown below, the effects of self-demagnetisation on induced magnetisation are analogous to those of anisotropy. Self-demagnetisation is a macroscopic phenomenon, applying to the magnetic body as a whole, whereas susceptibility anisotropy reflects the internal fabric or structure of the body.

A uniformly magnetised body is characterised by a demagnetising tensor, N, which relates the volume-averaged internal field, **H**, to the magnetisation, **J**, by the matrix equation (Brown, 1962)

$$\mathbf{H} = -N\mathbf{J}, \tag{18}$$

where **H** arises from the magnetic poles on the surface of the body. There is no volume distribution of poles because **J** is uniform, by assumption, so that div **J** = 0. The elements of N, N_{ij}, are coefficients of a linear relationship between the components of two vectors, **H** and **J**, i.e.

$$H_x = - N_{xx}J_x - N_{xy}J_y - N_{xz}J_z, \tag{19}$$

$$H_y = - N_{yx}J_x - N_{yy}J_y - N_{yz}J_z, \tag{20}$$

$$H_z = - N_{zx}J_x - N_{zy}J_y - N_{zz}J_z. \quad (21)$$

N is, by definition, a second order tensor. It can be shown that N is symmetric, i.e. $N_{ij} = N_{ji}$ for all i and j, so that it can be diagonalised. This means that three mutually orthogonal axes $\mathbf{u}_1$, $\mathbf{u}_2$, $\mathbf{u}_3$ can always be found such that N is diagonal with respect to these axes, i.e.

$$H_1 = - N_1J_1, \quad (22)$$

$$H_2 = - N_2J_2, \quad (23)$$

$$H_3 = - N_3J_3. \quad (24)$$

The principal components N_1, N_2, N_3 of the demagnetising tensor are known as demagnetising factors.

The principal axes $\mathbf{u}_1$, $\mathbf{u}_2$, $\mathbf{u}_3$ of simple bodies (of higher than monoclinic symmetry) coincide with the symmetry axes of the bodies. For example, the principal axes for a rectangular prism are parallel to the sides. The demagnetising field is uniform only for ellipsoidal bodies (including limiting cases of ellipsoids, such as spheres, infinite cylinders and infinite flat sheets), so that eqns (18)-(24) are exactly true at every internal point only for ellipsoids. For bodies of other shapes the relationships apply to the volume-averaged field, with local deviations due to inhomogeneity of the demagnetising field, particularly at corners and edges.

A second important property of demagnetising tensors is that the sum of the diagonal elements is invariant and equal to 4π in the cgs (emu or Gaussian) systems, or unity in SI, i.e.

$$N_{xx} + N_{yy} + N_{zz} = N_1 + N_2 + N_3 = 4\pi. \quad (25)$$

In the limit as one axis of a body becomes much greater than the others, the poles due to a magnetisation along that axis become effectively infinitely separated and the demagnetising field along the long axis approaches zero. Thus the demagnetising factor along the axis of a needle-shaped body is zero. Similarly, the demagnetising factors in the plane of a very thin disc or an infinite sheet are also zero. Demagnetising factors along other axes may sometimes be determined from eqn (25), coupled with symmetry considerations. Thus the demagnetising factors, along any three mutually orthogonal directions, of a sphere must be equal, by symmetry, and therefore must each be equal to $4\pi/3$, by (25). Similarly the demagnetising factors normal to the long axis of a needle-shaped body are equal to 2π and the demagnetising factor, $N_\perp$ normal to the plane of a thin disc or infinite sheet is 4π.

It follows from (22)-(24) that when the magnetisation lies along a principal axis of the demagnetising tensor the demagnetising field is antiparallel to the magnetisation. On the

other hand, when the magnetisation is oblique to the principal axes, **H** and **J** are not collinear.

Consider a magnetic body with intrinsic susceptibility k and intrinsic remanence $\mathbf{J}_r$ in an ambient field $\mathbf{H}_o$. The resultant internal field **H′** is then

$$\mathbf{H}' = \mathbf{H}_o + \mathbf{H} = \mathbf{H}_o - N\mathbf{J} = \mathbf{H}_o - N(\mathbf{J}_r + k\mathbf{H}'),$$

$$\therefore (I + kN)\mathbf{H}' = \mathbf{H}_o - N\mathbf{J}_r, \qquad (26)$$

where **J** is the resultant magnetisation (remanent + induced) and I is the unit matrix.

Solving (26) for **H′** gives

$$\mathbf{H}' = (I + kN)^{-1}(\mathbf{H}_o - N\mathbf{J}_r). \qquad (27)$$

From (26), the resultant magnetisation satisfies

$$(I + kN)\mathbf{J} = (I + kN)(k\mathbf{H}' + \mathbf{J}_r) = (k\mathbf{H}_o + \mathbf{J}_r),$$

$$\therefore \mathbf{J} = (I + kN)^{-1}(k\mathbf{H}_o + \mathbf{J}_r). \qquad (28)$$

The apparent remanence, $\mathbf{J}_r'$, is the magnetisation in zero applied field, i.e.

$$\mathbf{J}_r' = (I + kN)^{-1}\,\mathbf{J}_r. \qquad (29)$$

With respect to principal axes

$$(J_r')_i = (J_r)_i/(1 + kN_i), \qquad (i = 1,2,3) \qquad (30)$$

Therefore the remanence component along the $\mathbf{u}_i$ axis is attenuated by a factor of $1/(1 + kN_i)$ by the effect of self-demagnetisation. It follows from (30) that for an inequidimensional body (for which $N_1 \neq N_2 \neq N_3$), $\mathbf{J}_r'$ and $\mathbf{J}_r$ are not parallel, unless the remanence is directed along a principal axis. If not, the apparent remanence is deflected towards the axis with the smallest demagnetising factor (i.e. the longest axis), for which the attenuation by $1/(1 + kN)$ is least.

The induced magnetisation, $\mathbf{J}_{ind}$, corresponds to the term containing $\mathbf{H}_o$ in (28), i.e.

$$\mathbf{J}_{ind} = (I + kN)^{-1}\,k\mathbf{H}_o \qquad (31)$$

With respect to principal axes, (31) becomes

$$(J_{ind})_i = k(H_o)_i/(1 + kN_i) \qquad (32)$$

It follows from (32) that the induced magnetisation is only parallel to the applied field if $\mathbf{H}_o$ is directed along a principal axis. If not, the induced demagnetisation is deflected towards the longest axis, as for the remanence. From (32), if the applied

field is directed along a principal axis $\mathbf{u}_i$, so that J_{ind} is parallel to $\mathbf{H}_o = H_o\mathbf{u}_i$, then

$$J_{ind} = kH_o/(1 + kN_i),$$

$$\therefore\ k' = J_{ind}/H_o = k/(1 + kN_i), \qquad (33)$$

where k' is the apparent susceptibility. Thus the apparent susceptibility and the apparent remanence depend on the shape of the body, which determines the damagnetising factors, as well as on the intrinsic properties. This is important for determination of the intrinsic properties of samples in the laboratory, as mentioned in section 3, as well as for correct modelling of magnetic anomalies of high susceptibility bodies.

5. MAGNETIC MODELLING OF THE TROUGH TANK ANOMALY

Fig.17 shows the fundamental problem of interpreting magnetic anomalies arising from sheet-like bodies. Depending on the direction of magnetisation, 2D sheets with different dips can produce identical anomalies. The effective magnetisation for 2D structures is the projection of the total (induced + remanent) magnetisation onto the section normal to strike, because the along-strike component does not contribute to the field arising from the body. Equivalent dipping sheets are characterised by identical effective magnetisation-orthogonal thickness (Jt) products and by equal angles between the magnetisation and the plane of the sheet. This means that as the magnetisation and dip of a sheet rotate rigidly together the anomaly is unchanged, provided the magnetisation intensity is adjusted to maintain a constant Jt. A further interpretational ambiguity for thin sheets (those with thickness less than the depth to the top) is due to the impossibility of resolving magnetisation intensity and thickness separately, but this does not apply to thick sheets, for which, in principle, the top corners can be defined by modelling.

It follows from the equivalence of the dipping sheets of Fig.17 that interpretation of the dip requires additional knowledge or assumptions, in order to obtain a unique solution. The usual approach is to suppose remanence is negligible, or is dominated by VRM parallel to the present field, and to model the observed anomaly, assuming magnetisation parallel to the regional geomagnetic field. This is sufficient to determine the dip, provided the assumed direction of magnetisation is correct. In many cases dips have been misinterpreted due to the presence of significant remanence, with a direction oblique to the present field. Remanence is likely to be important, in particular, when the anomaly arises from pyrrhotite-bearing rocks, basic to acid volcanics or basic hypabyssal and plutonic rocks. In many rock types, however, the magnetisation tends to be predominantly induced (e.g. granitic rocks, sedimentary rocks, magnetite-bearing metasediments). In particular, rocks rich in coarse-grained magnetite, such as many massive magnetite ores, quartz-magnetite rocks and bifs, tend to have low Koenigsberger ratios

and soft remanences, often dominated by VRM. Such rocks, which produce large magnetic anomalies, therefore tend to be magnetised essentially by induction. The Starra and Trough Tank ironstones fall into this category, as seen in section 3.

Another factor which can affect interpreted dips is anisotropy of susceptibility. The deflection of induced magnetisation due to anisotropy is negligible for most rocks, for which the anisotropy degree is only a few percent, but can be important for rocks with A greater than about 2. Such rock types include many bifs and some pyrrhotite-bearing rocks and ores. The effect of very high anisotropy on the form of the anomaly over a dipping sheet, for which the susceptibility parallel to the sheet is much greater than the susceptibility normal to the sheet, is shown in Fig.18. The anomaly amplitude is sensitive to the dip of the sheet, but the shape of the B_T anomaly is independent of dip, except for a change of sign over a limited range of shallow northward dips. This is because the induced magnetisation is deflected into the plane of the sheet, whatever its orientation. Thus the magnetisation rotates with the sheet as the dip changes, in a similar way to a pre-folding remanence, with the difference that the magnetisation intensity is proportional to the component of **F** projected onto the plane of the sheet, $F_{=}$. Thus the amplitude of the B_T anomaly is proportional to $F_{=}t$. When the normal to the sheet becomes steeper than **F**, the sense of the induced magnetisation reverses and hence the anomaly changes sign.

Fig.18 shows that the dip of a very highly anisotropic sheet-like body cannot be determined from the anomaly, unless the susceptibility is known. For realistic values of anisotropy of bifs ($A \lesssim 4$), the induced magnetisation is deflected significantly, but not completely, towards the plane of the sheet. This means that the normal dip-dependence of the anomaly form is partially suppressed, but still detectable, so that dip can be correctly interpreted, provided the anisotropy is taken into account. The intrinsic susceptibility anisotropy of the Starra and Trough Tank quartz-magnetite ironstones is not very high (see section 3), because of the fairly massive nature of the magnetite. The ironstone units are macroscopically highly anisotropic, however, because of the high susceptibility and the sheet-like geometry, which produce strong self-demagnetisation. Thus the dip-dependence of the anomalies over such bodies is analogous to that associated with mesoscopically anisotropic bifs.

Given the above discussion, the erroneously interpreted dip at Trough Tank is therefore attributable neither to remanence nor to intrinsic, mesoscopic anisotropy. Two effects, both related to the very high susceptibility of the Trough Tank ironstone, account for the departure of the observed anomaly shape from that expected for a NE-dipping sheet:

(i) the large deflection of the induced magnetisation by self-demagnetisation, away from the present field direction towards the plane of the sheet,

(ii) the perturbation of the local field by the huge anomaly at Trough Tank, producing a significant distortion of the B_m anomaly compared to the shape predicted by standard B_T modelling.

Conventional modelling ignores points (i) and (ii), thereby making two assumptions which may be justified in most circumstances, but not in this case. These are:

Assumption (1) $\mathbf{J}_{ind}$ is parallel to $\mathbf{F}$,

Assumption (2) $B_m = B_T$.

Points (i) and (ii) above may be regarded as aspects of a single phenomenon: perturbation of the ambient field by a magnetic body. Self-demagnetisation reflects perturbation of the internal field and the difference between B_m and B_T arises from perturbation of the external field. Because the internal field arising from the magnetisation distribution is stronger, given favorable geometry, than the distant external field, it can be expected that the effects of self-demagnetisation may generally be more pronounced than those due to violation of assumption 2.

Line 1770N (Keel Grid) represents a typical profile across the Trough Tank anomaly, upon which the initial modelling was based. Fig.19 shows the observed 12,000 nT B_m anomaly and drilling information. The anomaly to be expected over the ironstones was calculated using MAGMOD 8B (Emerson et al., 1985), which can incorporate remanence, anisotropy and self-demagnetisation into the model. Assuming a susceptibility of 0.47 G/Oe (which is consistent with the measured values, given the variability in the deposit) the calculated anomaly amplitude, based on the simplest, geologically plausible model that fits the drilling intersections, agrees well with the observed anomaly and and the shape is approximately matched. Thus the general form of the anomaly is explained by the intersected material, with the correct NE dip.

The fit to the observed anomaly can be improved by adjusting the model, increasing the susceptibility of the SW sheet and decreasing the susceptibility and increasing the width of the NE sheet. Such a model would still be consistent with the mid-range of measured susceptibilities and with the drilling intersections. However the simple model of Fig.19 suffices to confirm the approximate agreement between the observed and predicted B_m anomalies over Trough Tank, when self-demagnetisation is incorporated into the model. Because remanence only makes a minor contribution to the magnetisation of the Trough Tank samples, it was not considered worthwhile to incorporate it into the simple models, which are designed to illustrate the most important factors for interpretation of this anomaly. The modelling also does not take into account the finite strike length and the effect of interaction between the bodies, obviating the utility of fitting the anomaly very closely.

A variation of the simplest model, which incorporates the effect of possible mesoscopic banding of the ironstones on a scale larger than the measured specimens, was also investigated. Such banding produces an effective macro-anisotropy which would not show up in the anisotropy of individual specimens. Assuming the ironstone units consist of very magnetite-rich bands with susceptibility equal to 1 G/Oe (47%), separated by non-magnetic bands (53%), results in a parallel susceptibility equal to the isotropic intrinsic susceptibility of the simple model, i.e.

$$k'_{=} = k_{=} = 0.47 \text{ G/Oe},$$

and an effective perpendicular susceptibility of

$$k'_{\perp} = 0.47 \times 1/(1 + 4\pi \times 1) = 0.035 \text{ G/Oe}.$$

According to eqn (2), this corresponds to an intrinsic perpendicular susceptibility of

$$k_{\perp} = 0.035/ (1 - 4\pi \times 0.035) = 0.061 \text{ G/Oe}.$$

Thus the intrinsic anisotropy of the unit arising from self-demagnetisation of the individual postulated bands is A = 0.47/0.061 = 7.7 and the effective anisotropy, including the effect of self-demagnetisation of the unit as a whole, is A′ = 0.47/0.035 = 13.6. This compares with the effective anisotropy of the simple model, which is intrinsically isotropic, for which

$$k'_{=} = k_{=} = 0.47; \; k'_{\perp} = 0.47/(1 + 4\pi \times 0.47) = 0.068,$$

$$\therefore A' = 0.47/ 0.068 = 6.9.$$

It can be seen from Fig.19 that the predicted anomaly agrees somewhat better with the observed anomaly when the above values of parallel and perpendicular susceptibility pertaining to a banded unit are used in the model. An estimated upper limit for the intrinsic anisotropy due to banding can be obtained by assuming that all the variability in measured susceptibility values arises from representative sampling of different, laterally perfectly homogeneous thin sheets. Then the average parallel susceptibility remains equal to 0.47 G/Oe, because self-demagnetisation in the plane of the sheets is zero, but the effective perpendicular susceptibility is equal to the average of the demagnetisation-corrected perpendicular susceptibilities. The value obtained is $k_{\perp}$ = 0.061 G/Oe (which corresponds to A′= 7.7). This is less than the demagnetisation-corrected value of the average susceptibility, because of the non-linear relationship (33) between intrinsic and demagnetisation-corrected susceptibilities. This analysis suggests that the correct intrinsic anisotropy of the units lies between the values used in the models of Fig.19 and the corresponding calculated anomaly should therefore plot between the two theoretical curves.

The effects of non-linear superposition are also apparent

from Fig.19. The true B_m anomaly arising from the two sheets jointly plots above the sum of the individual B_m anomalies. The difference is quite small in this case, however. Effects of comparable magnitude are to be expected from the interaction between the two units. This latter effect arises from the fact that the field within each body is perturbed by the other, nearby, strongly magnetic body, so that the induced magnetisation is modified. Because the anomalous field within each body is non-uniform, this effect cannot be simply incorporated into the model by modifying the model magnetisation, which is assumed to be uniform. Correction for this second order effect involves iteratively solving a discretised integral equation for the non-uniform internal fields and magnetisation distributions (Eskola and Tervo, 1980). The same approach is needed in order to correct for non-uniform self-demagnetising fields near the corners of the sheets. Theoretical calculations and analogue modelling studies (Hjelt and Phokin, 1981) indicate that distortion of the anomaly due to interactions and non-uniform self-demagnetising fields should be fairly minor at Trough Tank, although these factors are quite important for susceptibilities as high as those of the Starra quartz-magnetites.

The errors associated with assumptions (1) and (2) can best be evaluated using a simplified, isotropic single sheet model. This is quite a reasonable representation of the source, since the two units are only just resolved by the ground magnetics, and the principles involved can be discussed more clearly in the context of a simple geometry. Fig.20 illustrates the deflection of induced magnetisation due to self-demagnetisation, for the geometry of Trough Tank. Note that for 2D bodies the along strike component of magnetisation does not contribute to the anomalous field. The effective regional geomagnetic field (i.e. the projection of **F** onto the vertical section normal to strike) makes an angle of 73^o with the up-dip direction. The parallel susceptibility is simply the intrinsic susceptibility, k, because the demagnetising factor in the plane of the sheet is zero. On the other hand the perpendicular susceptibility is attenuated by $1/(1 + 4\pi k)$. Resolving **F** and **J** into up-dip and perpendicular components as shown, it can be seen that the induced magnetisation is deflected towards the plane of the sheet, such that the angle between the effective magnetisation and the up-dip direction is

$$\alpha = \tan^{-1}[\tan 73^o/(1 + 4\pi k)]. \qquad (34)$$

The equivalent sheet with magnetisation parallel to **F** is shown dashed in Fig.20. The angle of deflection, ,is equal to the error in the apparent dip interpreted from component-type anomalies, as shown in Fig.17. Thus, ignoring the difference between B_m and B_T for the moment, the error in interpreted dip to be expected from neglecting self-demagnetisation is

$$\delta = 73^o - \tan^{-1}[\tan 73^o/(1 + 4\pi k)]. \qquad (35)$$

Values of dip error for various values of k are listed in Table

7. The magnitude of the error is a highly non-linear function of susceptibility. For low susceptibilities the error is negligible ($< 2^{o}$ for $k < 0.01$ G/Oe), but increases rapidly for susceptibilities above ~0.1 G/Oe. The rate of increase in the error levels off above k ~1 G/Oe, and approaches an upper limit of 73^{o} (corresponding to induced magnetisation deflected completely into the plane of the sheet) as k increases without limit. For the mean measured susceptibility of the Trough Tank ironstone samples ($k = 0.58$ G/Oe) the error is 51^{o} and for the interpreted susceptibility derived from modelling ($k = 0.47$ G/Oe), the error is 48^{o}. Such an error is likely to severely mislead drill targetting. The maximum possible errors in interpreted dip, corresponding to the most favourable geometry for deflection of induced magnetisation, are also given in Table 7 as a function of susceptibility. It can be seen that the geometry at Trough Tank produces a deflection almost as large as the maximum possible. More magnetic bodies, typified by susceptibilities comparable to the average of the Starra ironstone samples, can deflect induced magnetisation by almost as much as a sheet with infinite susceptibility.

The dip error discussed above applies to interpretation of the B_m anomaly at a height above the body sufficient to ensure that $B_m \ll F$, so that $B_m \sim B_T$. For the ground magnetic anomaly at Trough Tank the difference between B_m and B_T is substantial. Fig.21 shows a comparison of the B_m and B_T anomalies for dipping sheets comparable in thickness and susceptibility to the Trough Tank ironstones. For each geometry the difference is greatest along the steep gradient on the SW flank of the anomaly, where the anomalous field vector, **B**, is large and is approximately perpendicular to the effective geomagnetic field. The difference between B_m and B_T is smaller along the NE flank of the anomalies, because here **B**, although large, is subparallel to the effective field, so the resultant field direction is not deflected as much from the regional field direction. The absolute difference between the two types of anomaly is greatest for the vertical sheet, largely reflecting the greater magnitude of the anomalous field over this sheet, for which the orthogonal thickness is greatest. The magnetisation of the SW-dipping sheet is the highest, accounting for the much larger anomaly over it than over the NE-dipping sheet, but the magnetisation-orthogonal thickness product is slightly less than the corresponding value for the vertical sheet.

The controlling influence of self-demagnetisation can be judged from the fact that the difference in anomaly amplitude between the NE-dipping and SW-dipping sheets in Fig.5 entirely reflects self-demagnetisation. Bodies dipping 45^{o} NE and 45^{o} SW with $k = 0.001$ G/Oe, say, would have practically identical induced magnetisations and total anomaly amplitudes (measured peak-to-trough), but very different anomaly shapes, with a much more pronounced low (to the SW) for the NE-dipping sheet than for the SW-dipping sheet. When self-demagnetisation is important, however, the induced magnetisation is greatly attenuated if the effective field is at a large angle to the plane of the sheet, as

for the NE-dipping sheet, but less attenuated for SW dips with the effective field subparallel to the sheet. On the other hand, the dip-dependence of anomaly shape is suppressed by self-demagnetisation, because the induced magnetisation tends to rotate with the sheet as the dip changes.

Although the dip-dependence of anomaly shape is more subtle in Fig.5 than for corresponding weakly magnetic sheets, the dips are nevertheless interpretable, provided the susceptibility can be estimated and self-demagnetisation is included in the analysis. The susceptibility can be determined, in principle, by modelling the location of the top corners of the sheet and matching the anomaly amplitude with the appropriate value of demagnetisation-corrected induced magnetisation x orthogonal thickness product, which is dip-dependent. This can only be accomplished uniquely for thick sheets, as no information on sheet thickness can be derived from the anomaly if t << h.

It is evident from Fig.21 that the B_m anomaly lies above the B_T anomaly, in agreement with (15), and that for B_m the anomaly minimum to the SW is suppressed and the gradient on the SW flank is flattened compared to the corresponding features in the B_T anomaly. These effects imply that the apparent dip of the sheet, as interpreted by matching the observed B_m with a calculated B_T, is rotated towards the SW, i.e. the interpretational error due to neglecting the difference between B_m and B_T adds to the dip error from neglecting self-demagnetisation. Fig.22 shows the separate and combined effects of points (i) and (ii) above on the apparent dip of a bif unit comparable to Trough Tank. The anomalies plotted in Fig.22 are normalised to facilitate comparison of anomaly shapes. Conventional modelling of a sheet dipping 45° NE, neglecting self-demagnetisation and the difference between B_m and B_T, produces a dipolar anomaly shape with a very pronounced low to the SW. For a susceptibility of 0.1 G/Oe, self-demagnetisation significantly reduces the size of the low relative to the anomaly high. The resulting anomaly shape resembles that of a low susceptibility body with a dip of 63° NE. For a susceptibility of 0.5 G/Oe the B_T anomaly corresponds to an apparent dip of 86° SW, but the B_m anomaly shape corresponds approximately to the shape of the B_T anomaly from a sheet with a dip of $\sim 81^{\circ}$ SW. Thus the effect of neglecting the difference between B_m and B_T is an additional dip error of about 5° for the Trough Tank ironstone, which is minor compared to the effect of neglecting self-demagnetisation. The effect of mesoscopic banding or macroscopic sheet-like zoning on the anomaly shape is also shown for the case where the body consists of 50% high susceptibility (1 G/Oe) bands separated by non-magnetic bands. This corresponds to a parallel susceptibility of 0.5 G/Oe with an effective perpendicular susceptibility of 0.0369 G/Oe, or an intrinsic perpendicular susceptibility of 0.0687 G/Oe. The induced magnetisation for this case is parallel to the induced magnetisation of a homogeneous body with k = 1 G/Oe, i.e. it is deflected by 59° and therefore contributes 59° to the dip error. Thus the difference between the curves for the anisotropic, banded body and the homogeneous body

with k = 1 G/Oe reflects only the greater anomaly amplitude, and the consequently greater perturbation of the geomagnetic field, for the latter case. The anomaly shape changes only slowly with increasing susceptibility for k > 1 G/Oe. The relative contribution of the error from neglecting the difference between B_m and B_T becomes increasingly important for increasing k, because the distortion of the ambient field becomes greater as the anomaly amplitude increases. This is reinforced by the suppression of the dip-dependence of anomaly shape due to deflection of the induced magnetisation, which becomes more subtle as the magnetisation approaches the plane of the sheet.

6. CONCLUSIONS

(i) The Starra and Trough Tank ironstones are characterised by very high susceptibilities (~1.7 G/Oe for Starra and ~0.5 G/Oe for Trough Tank) which produce substantial self-demagnetising effects. Remanence makes a minor contribution to the intrinsic magnetisation of the ironstones. The effective Koenigsberger ratio for these bodies is ~0.2. The effective remanence of both bodies is directed steep up, although both polarities of remanence are found at Trough Tank, and is probably ancient. The intrinsic anisotropy arising from the banding of these ironstones is quite small ($A \simeq 1.1$), at least on a specimen scale, and does not, in itself, significantly deflect the direction of induced magnetisation. The low anisotropy reflects the fairly massive nature of these bifs, compared to Hamersley bifs, for instance.

(ii) The geometry of the Trough Tank ironstones is conducive to producing large self-demagnetising effects. The induced magnetisation of the ironstones is deflected significantly towards the plane of the sheet-like units, because the effective susceptibility perpendicular to the plane of the sheets is greatly attenuated with respect to the susceptibility parallel to the sheets. The magnitude of the deflection is about 50° for the Trough Tank ironstones, which corresponds to a ~50° error in the interpreted dip, if self-demagnetisation is not included in the modelling program.

(iii) Conventional magnetic modelling calculates the "total field" anomaly as the projection of the anomalous field vector, produced by the magnetic body, onto the regional geomagnetic field direction. This is equivalent to assuming that the deflection of the local geomagnetic field by the anomaly is negligible, which is a very good approximation in most circumstances. When the anomaly represents a significant proportion of the geomagnetic field, however, this assumption breaks down. Calculation of the anomaly corresponding to what is

actually measured by a total field magnetometer is an elementary exercise and all software for magnetic modelling should be modified accordingly, in order to eliminate possible interpretational errors for large anomalies. It may also be necessary to modify processing software for upward/downward continuation, reduction to the pole, derivative calculations etc., in order to correct for deviations of the measured field from the potential field approximation, which assumes that the anomalies represent directional derivatives, along the regional geomagnetic field direction, of the magnetic scalar potential.

(iv) At Trough Tank the ground magnetic anomaly has maximum amplitude of ~15,000 nT, which is a substantial fraction of the geomagnetic field. Thus the local anomaly significantly deflects the resultant field direction and distorts the form of the measured scalar (B_m) anomaly with respect to the conventionally calculated total field anomaly (B_T). The additional error in interpreted dip due to ignoring the difference between B_m and B_T is about 5^o, which is relatively minor. This effect, however, becomes increasingly important with proximity to such highly magnetic bodies.

7. ACKNOWLEDGEMENTS

Cyprus Minerals Australia kindly contributed the Starra samples. I thank Peter Gidley of CSR Ltd for initiating this study and for helpful discussions.

8. REFERENCES

Backus, G.E., 1968. Application of a non-linear boundary-value problem for Laplace's equation to gravity and geomagnetic intensity surveys. Quart. J. Mech. and Appl. Math., **21**, 195-221.

Blake, D.H., 1987. Geology of the Mount Isa Inlier and environs, Queensland and Northern Territory. BMR Bulletin 225.

Blake, D.H., Jaques, A.L. and Donchak, P.J.T., 1983. 1:100 000 Geological Map Commentary, Selwyn Region, Queensland. BMR and Geol. Surv. Qld.

Blake, D.H., Bultitude, R.J., Donchak, P.J.T., Wyborn, L.A.I. and Hone, I.G., 1984. Geology of the Duchess-Uranangi region, Mount Isa Inlier, Queensland. BMR Bulletin 219.

Brown, W.F., 1962. Magnetostatic Principles in Ferromagnetism. North-Holland, Amsterdam, 202 pp.

Clark, D.A., 1979. Applied Magnetic Interpretation Symposium - Discussion. Bull. Aust. Soc. Explor. Geophys., **10**, 131-135.

Clark, D.A., 1986. Magnetic and gravity anomalies of a triaxial ellipsoid.Exploration Geophysics, **17**, 189-200.

Clark, D.A., 1988. Magnetic fabric - principles and applications to tectonics. Ninth Australian Geological Convention. Geol. Soc. Australia Abstracts, **21**, 90-92.

Clark, D.A. and Embleton, B.J.J., 1980. Applications of rock magnetism. CSIRO Restricted Investigation Report 1193R.

Clark, D.A., Emerson, D.W. and Kerr, T., 1987. The use of electrical conductivity and magnetic susceptibility tensors in rock fabric studies. Explor. Geophys., **19**, 244-248.

Clark, D.A. and Schmidt, P.W., 1986. Geological structure and magnetic signatures of Hamersley bifs. CSIRO Restricted Investigation Report 1639R.

Collins, S., 1987. The geophysics of the Starra gold/copper deposits. Exploration Geophysics, **18**, 20-22.

Davidson, G.J., 1987. Starra and Trough Tank Au-Cu deposits: oxide mineralisation in a shallow intracratonic setting. In: Geology and Geochemistry of Gold-Copper Iron Oxide Systems: Tennant Creek and Starra Districts. Workshop Manual No. 1, Tennant Creek, July 1987. University of Tasmania.

Davidson, G., Large, R., Kary, G. and Osborne, R., 1988. The bif-hosted Starra and Trough Tank Au-Cu mineralisations: a new stratiform association from the Proterozoic Eastern Succession of Mt Isa, Australia. Bicentennial Gold 88 Conference, Melbourne, Extended Abstracts.

Emerson, D.W., Clark, D.A. and Saul, S.J., 1985. Magnetic exporation models incorporating remanence, demagnetization and anisotropy: HP41C handheld computer algorithms. Exploration Geophysics, **16**, 1-122.

Eskola, L. and Tervo, T., 1980. Solving the magnetostatic field problem (a case of high susceptibility) by means of the method of subsections. Geoexploration, **18**, 79-95.

Gidley, P.R., 1988. The geophysics of the Trough Tank Gold-Copper Prospect, Australia. Exploration Geophysics, **19**, 76-78.

Hughes, D.S. and Pondrom, W.L., 1947. Computation of vertical magnetic anomalies from total magnetic field anomalies. Trans. Am. Geophys. Union, **28**, 193-197.

Hjelt, S.O., and Phokin, A.P., 1981. Interpretation of borehole magnetic data and some special problems of magnetometry. Dept of Geophysics, Univ. of Oulu, Finland, Rep. No. 1, 177 pp.

Kontis, A.L. and Young, G.A., 1964. Approximation of residual total-magnetic-intensity anomalies. Geophysics, **29**, 623-627.

Laing, W.P., Rubenach, M.J. and Switzer, C.K., 1988. The Starra gold-copper deposit - syndeformational metamorphic mineralisation localised in a folded early regional zone of decollement (abstract). Ninth Australian Geological Convention. Geol. Soc. Australia Abstracts, **21**, 229.

Mock, C.M., Lorenz, R.P. and Elliott, B.G., 1988. Gold deposits of Queensland: BMR Datafile (MINDEP).

Morrison, I., 1986. The Starra Au-(Cu) project, N.W. Queensland. In: Gold Exploration and Development, North Queensland Conference, Charters Towers. Aus. I.M.M.

Ridley, B.H. and Brown, H.E., 1980. The transformer bridge and magnetic susceptibility measurement. Bull. Aust. Soc. Explor. Geophys., **11**, 110-114.

Schmidt, P.W. and Clark, D.A., 1985. Presentation and analysis of palaeomagnetic data. CSIRO Restricted Investigation Report 1602R.

Table 1. List of samples from the Starra deposit.

Sample DDH	Depth (m)	Description
DEC		oriented block sample of quartz-haematite (oxidised bif) from the Starra decline
STQ-87-253	203.5	black, qtz-mt rich ironstone (qtz-hm-mt-cp), 1a type, mt 15-20% as 0.5-5 mm euhedral grains in bands or clusters elongate parallel to the schistosity. cp 5%, py 1%, hm 20% approximately.
"	206.85	grey, qtz-mt rich, ironstone as above.
STQ-86-216	209.9	silver grey brecciated ironstone (mt-qtz-cp-hm), mt 0.5 -5 mm diameter, commonly 1-2 mm, 20-40%, foliated within qtz-hm matrix. Foliation is parallel to schistosity.
STQ-87-254	284.0	dark grey, qtz-mt ironstone, banded parallel to the schistosity. Fine-medium grained euhedral mt within very fine grained qtz matrix, with siderite and traces of chalcocite.
STQ-85-126/W	324.1	grey-black qtz-mt rich ironstone (medium-coarse grained mt, 25-35%, as blebs up to 3 mm diameter, plus fine grained qtz), with cp, py.
STQ-85-134	344.9	black mt-qtz ironstone: massive coarse grained mt (60%), with fine interstitial qtz + calcite (1%) + cp (up to 1%).

qtz = quartz, mt = magnetite, hm = haematite, cp = chalcopyrite, py = pyrite

Table 2. List of samples from Trough Tank.

Sample DDH	Depth (m)	Description
TTNQ3	61.2	banded qtz-hm-mt + py + cp
"	70.6	banded qtz-mt-hm
"	75.1	banded qtz-mt-hm
"	86.9	banded (slightly brecciated) qtz-mt-hm + cp
"	92.3	massive (slightly banded) qtz-mt + sulphides
"	105.9	pegmatite/ qtz-feldspar schist
"	114.1	pegmatite grading to qtz-mt
"	125.9	banded qtz-mt + sulphides
"	141.2	qtz-feldspar schist
"	144.6	qtz-feldspar schist
TTNQ4	102.1	very coarse grained (up to 4 mm), highly contorted, mt-qtz-hm + sulphides
"	104.8	banded qtz-mt grading to recrystallised feldspathic quartzite
"	115.1	highly contorted, medium-coarse grained mt-qtz-hm with phlogopite schist bands
"	122.9	banded mt-qtz-hm
"	132.9	fine grained, semi-massive mt-qtz-hm
"	135.9	brecciated qtz-mt + sulphides
"	140.1	highly contorted, brecciated qtz-mt + sulphides
TTNQ6	84.6	banded qtz-mt-hm + sulphides
"	89.9	banded qtz-mt-hm + sulphides
"	103.4	banded qtz-hm-mt + sulphides

Table 2 (continued).

TTNQ6	108.7	contorted banded/brecciated qtz-mt + sulphides
"	114.4	contorted banded/brecciated qtz-mt + sulphides

Symbols as for Table 1.

Table 3. Susceptibility, NRM and Koenigsberger ratio of Starra samples.

Sample	k (G/Oe)	NRM (Int(G);Dec,Inc)	Q
DEC	0.00563	(0.00184;034°,-28°	0.62
203	0.302	(0.148;101°,-78°)	0.93
206	0.672	(0.426;122°,-79°)	1.21
209	0.193	(0.061;097°,-43°)	0.60
284	2.555	(0.111;126°,-23°)	0.08
324	0.662	(0.154;162°,-47°)	0.44
344	6.023	(0.358;082°,-39°)	0.11
qtz-mt combined	1.735	(0.189;108°,-60°)	0.21

k = bulk cgs(emu) susceptibility (SI susceptibility = k x 12.56).
NRM intensity is expressed in Gauss (1G = 1 kA/m, SI).
Declination is measured positive clockwise from true north, inclination is positive downwards.

Table 4. Susceptibility, NRM and Koenigsberger ratio of Trough Tank samples.

Sample	k (G/Oe)	NRM (Int(G);Dec,Inc)	Q
NQ3 61	0.122	(0.001;294°,+37°)	0.02
NQ3 70	0.843	(0.201;026°,-27°)	0.45
NQ3 75	0.677	(0.190;018°,-46°)	0.53
NQ3 86	0.578	(0.127;140°,-26°)	0.42
NQ3 92	1.042	(0.226;019°,-14°)	0.41
NQ3 114	0.139	(0.073;254°,-38°)	1.00
NQ3 125	0.555	(0.072;202°,-07°)	0.25
NQ4 102	1.421	(0.016;035°,-49°)	0.02
NQ4 104	0.176	(0.007;301°,-08°)	0.08
NQ4 115	0.128	(0.011;138°,-24°)	0.16
NQ4 122	1.579	(0.326;014°,-63°)	0.39
NQ4 132	0.393	(0.020;283°,+51°)	0.09
NQ4 135	0.247	(0.017;016°,-20°)	0.13
NQ4 140	5.35×10^{-3}	(0.003;348°,-45°)	1.10
NQ6 84	0.630	(0.013;288°,-58°)	0.03
NQ6 89	0.340	(0.066;278°,+40°)	0.37
NQ6 103	0.063	(0.005;095°,-65°)	0.16
NQ6 108	0.880	(0.202:090°,-49°)	0.44
NQ6 114	1.189	(0.030;109°,-26°)	0.05
qtz-mt combined	0.579	(0.054;033°,-55°)	0.18

Table 4 (continued).

NQ3 105	1.2×10^{-5}	$(3.1 \times 10^{-6}; 004^{\circ}, -44^{\circ})$	0.49
NQ3 141	3.2×10^{-5}	$(9.6 \times 10^{-6}; 026^{\circ}, -77^{\circ})$	0.57
NQ3 144	1.6×10^{-5}	$(0.5 \times 10^{-6}; 037^{\circ}, -17^{\circ})$	0.05
all samples combined	0.478	$(0.046; 033^{\circ}, -55^{\circ})$	0.18

Symbols as for Table 3.

Table 5. Maximum difference between B_m and B_T, E_{max}, as a function of anomaly amplitude (B) and geomagnetic intensity (F).

B (nT)	1000	5000	10,000	15,000	20,000
F (nT)					
30,000	17	417	1667	3750	6667
35,000	14	357	1429	3214	5714
40,000	13	313	1250	2813	5000
45,000	11	278	1111	2500	4444
50,000	10	250	1000	2250	4000
55,000	9	227	909	2045	3636
60,000	8	208	833	1875	3333
65,000	8	192	769	1731	3077
70,000	7	179	714	1607	2857

Table 6. Contrasting mathematical properties of B_m and B_T.

PROPERTY	B_T	B_m
Definition	Projection of anomalous field vector $\mathbf{B} = \mathbf{F}' - \mathbf{F}$ onto direction of regional geomagnetic field: $B_T = \mathbf{B}.\mathbf{F}/\lvert\mathbf{F}\rvert$	Measured total field anomaly, equal to difference between local field intensity and regional field intensity: $B_m = \lvert\mathbf{F}'\rvert - \lvert\mathbf{F}\rvert$
Potential field?	YES	NO
Laplacian	div grad $(B_T) \equiv 0$	div grad $(B_m) \neq 0$
Validity of linear filtering for:		
up/down continuation	VALID	INVALID
vertical derivatives	"	"
reduction to pole	"	"
anomaly components	"	"
pseudogravity transformation	"	"
apparent susceptibility mapping	"	"
Multiple sources	Obeys linear superposition	Does not obey linear superposition
Anomaly shape	Independent of magnetisation intensity	Depends on intensity of magnetisation
Anomaly amplitude	Proportional to magnetisation intensity	Not proportional to intensity of magnetisation

Table 7. Deflection of induced magnetisation due to self-demagnetisation (Trough Tank geometry).

Susceptibility (G/Oe)	Deflection (Trough Tank geometry)	Maximum deflection
0.0	0°	0°
0.01	2°	3°
0.05	9°	14°
0.1	18°	23°
0.2	30°	34°
0.5 (≈ Trough Tank)	49°	49°
1.0	59°	60°
1.7 (≈ Starra)	65°	66°
2.0	66°	68°
3.0	68°	72°
5.0	70°	76°
10.0 (upper limit for massive, coarse-grained, well-annealed magnetite)	72°	80°
THEORETICAL UPPER LIMITS		
infinity	73°	90°

Fig.1. Regional geology and location of the Starra and Trough Tank deposits.

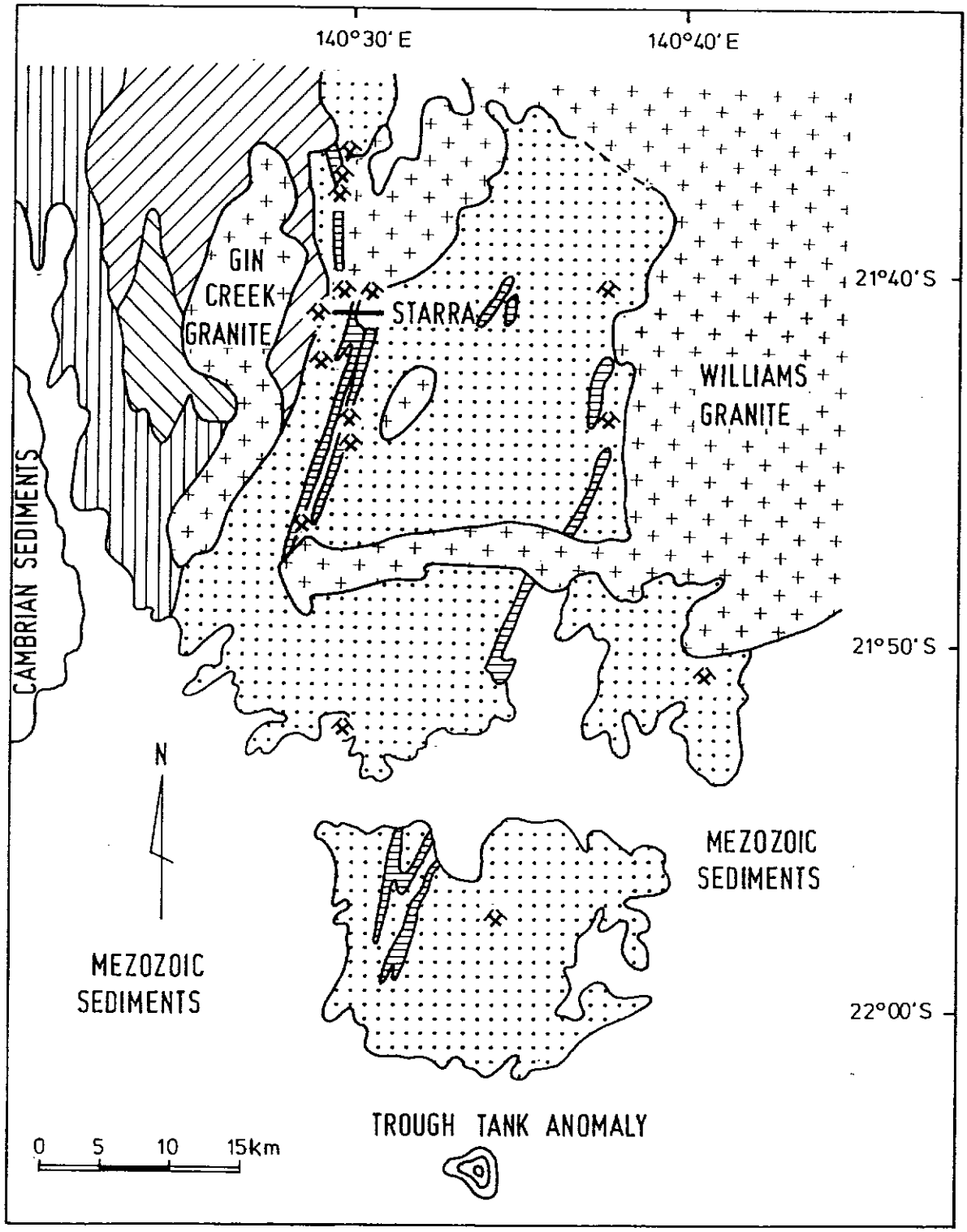

FIG. 1 GEOLOGY OF THE STARRA - TROUGH TANK AREA

Williams Batholith

Metadolerite, Amphibolite

Staveley Formation

Kuridala Formation

Answer Slate

Double Crossing Metamorphics

Fig.2. NRM directions of unoxidised bif specimens from Starra.

STARRAFC.rem NRM

203
206
209
284
324
344

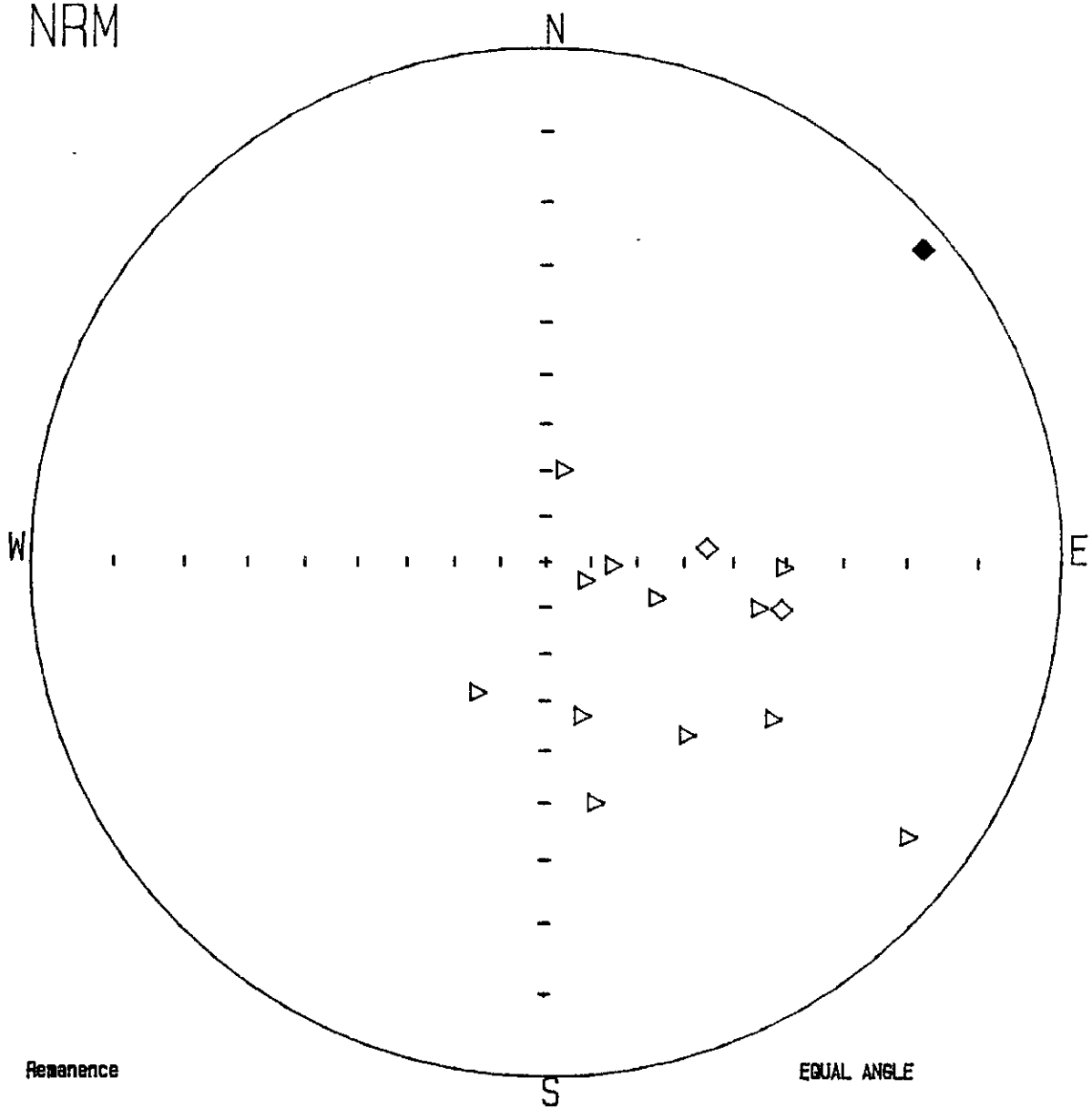

Fig.3. NRM directions of specimens from the oxidised bif sample, Starra decline.

STARRAFC.rem NRM

DEC

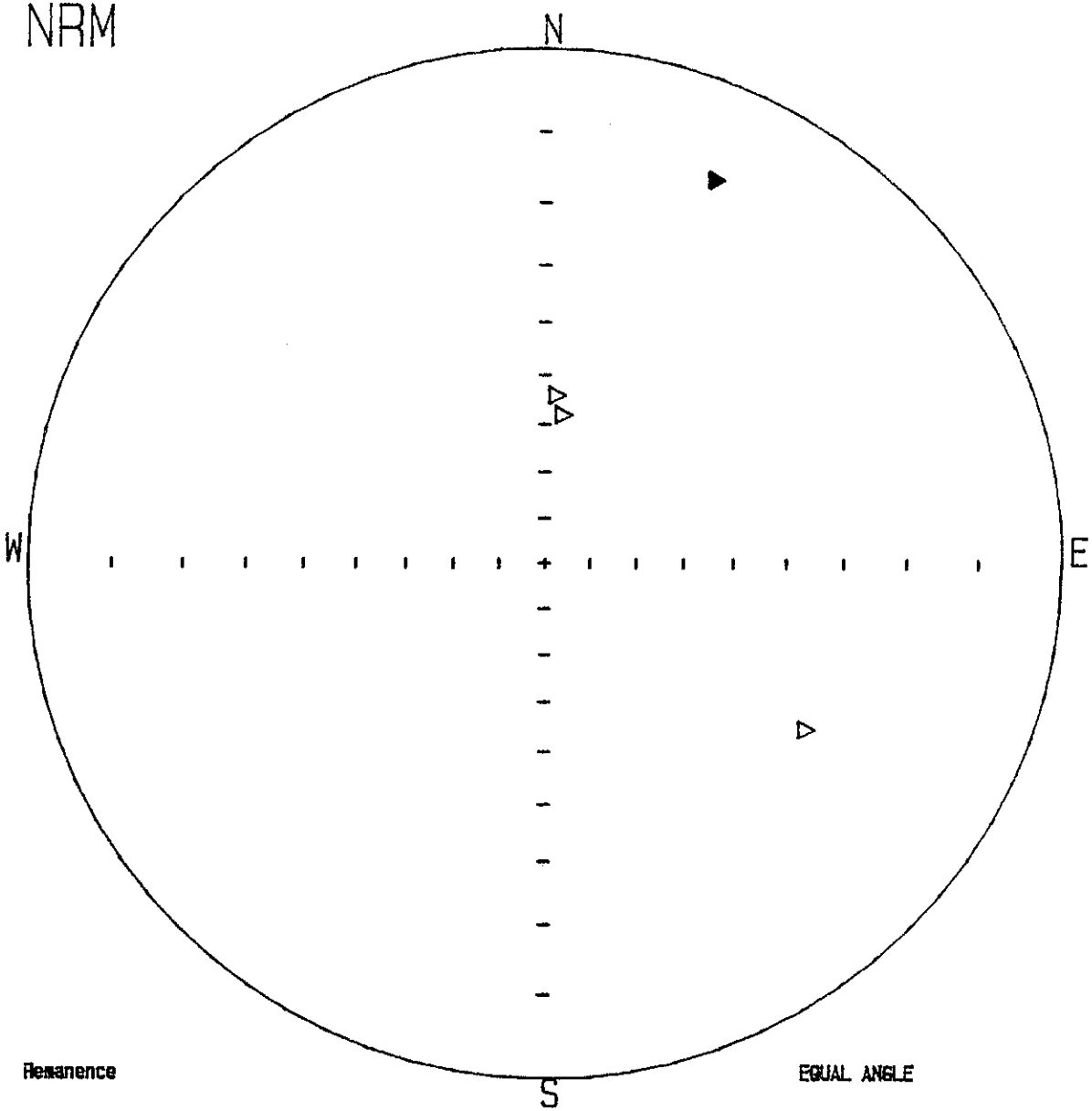

Fig.4. NRM directions of all specimens from the Trough Tank prospect.

TTANKFC.rem NRM

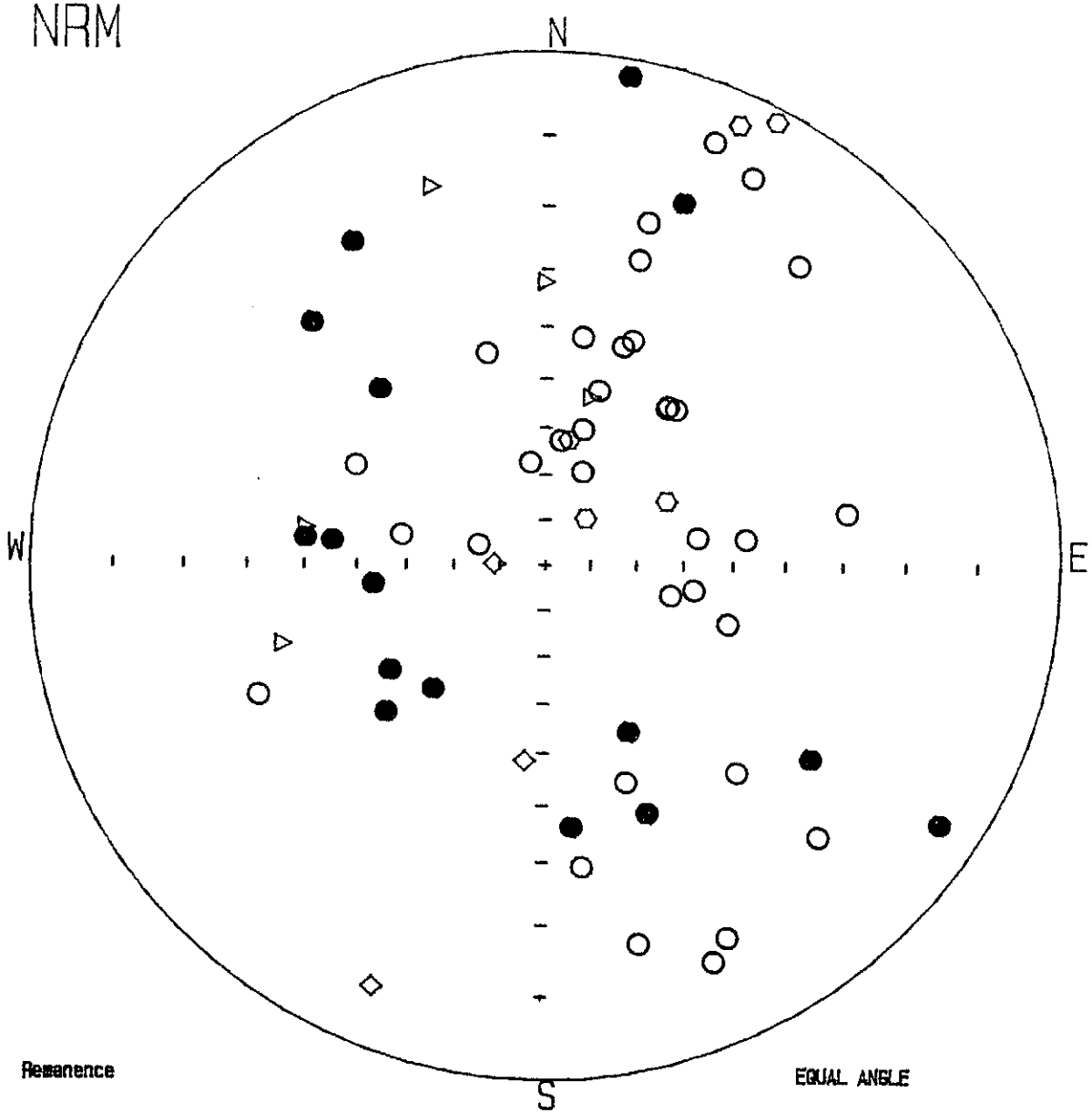

Fig.5. AF (200 Oe) cleaned remanence directions for Starra quartz-magnetite specimens.

STARRAFC.rem

200 0E

203
206
209
284
324
344

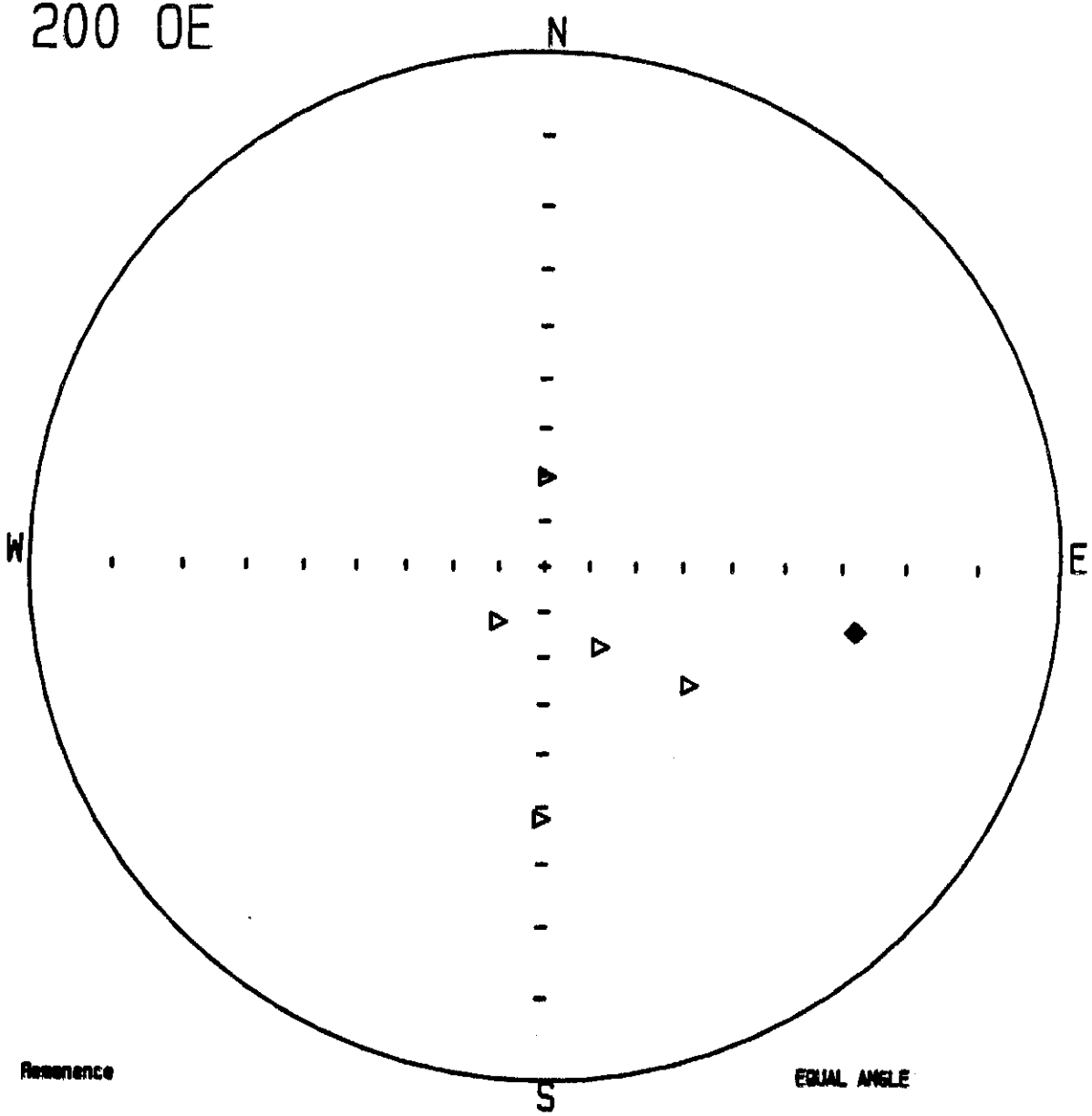

Fig.6. Thermal (550°C) cleaned remanence directions for Starra quartz-magnetite specimens.

STARRAFC.rem 550C

203
206
209
284
324
344

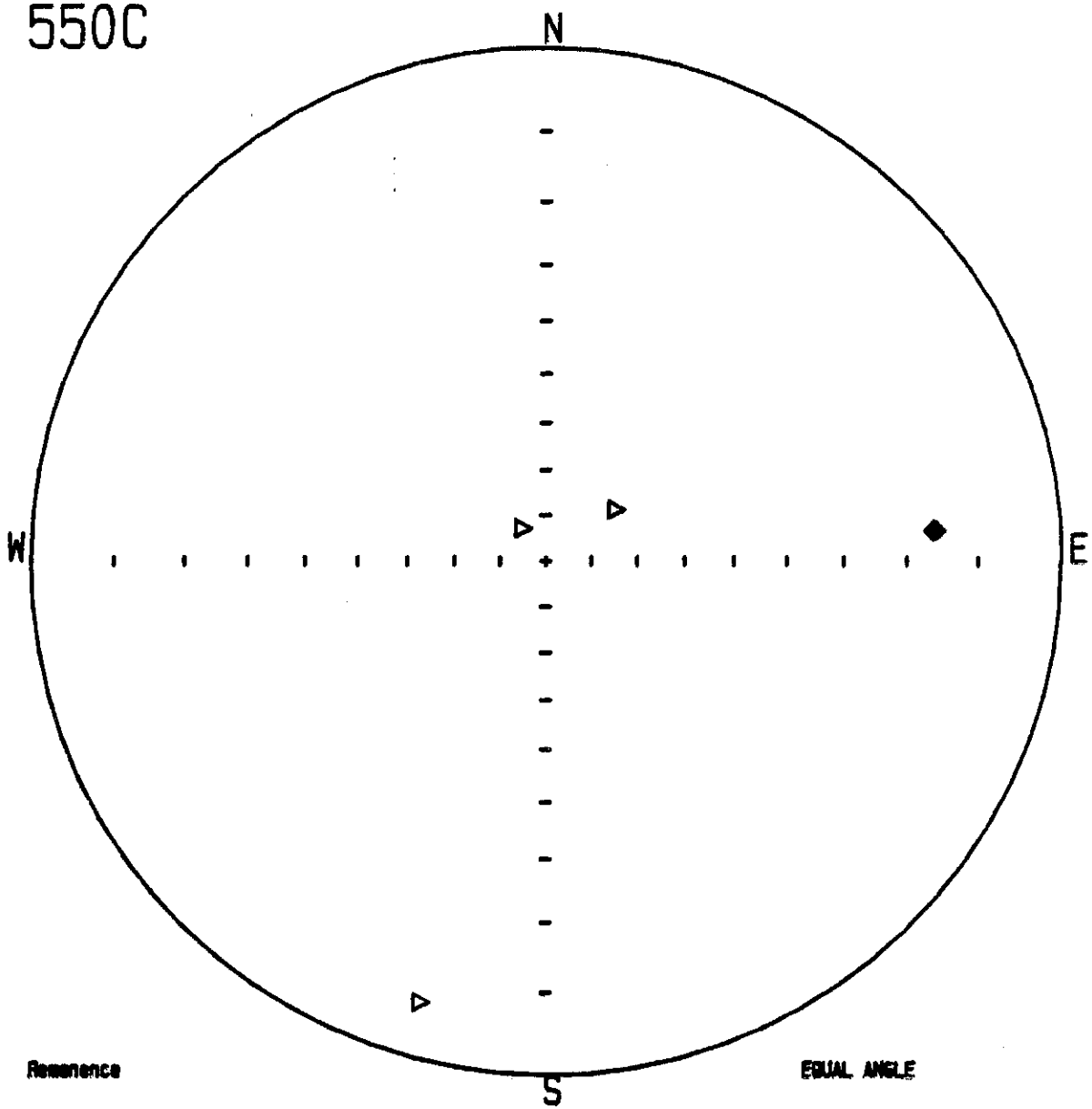

Fig.7. AF (140 Oe) cleaned remanence directions for Trough Tank bif specimens.

TTANKFC.rem 140 0E

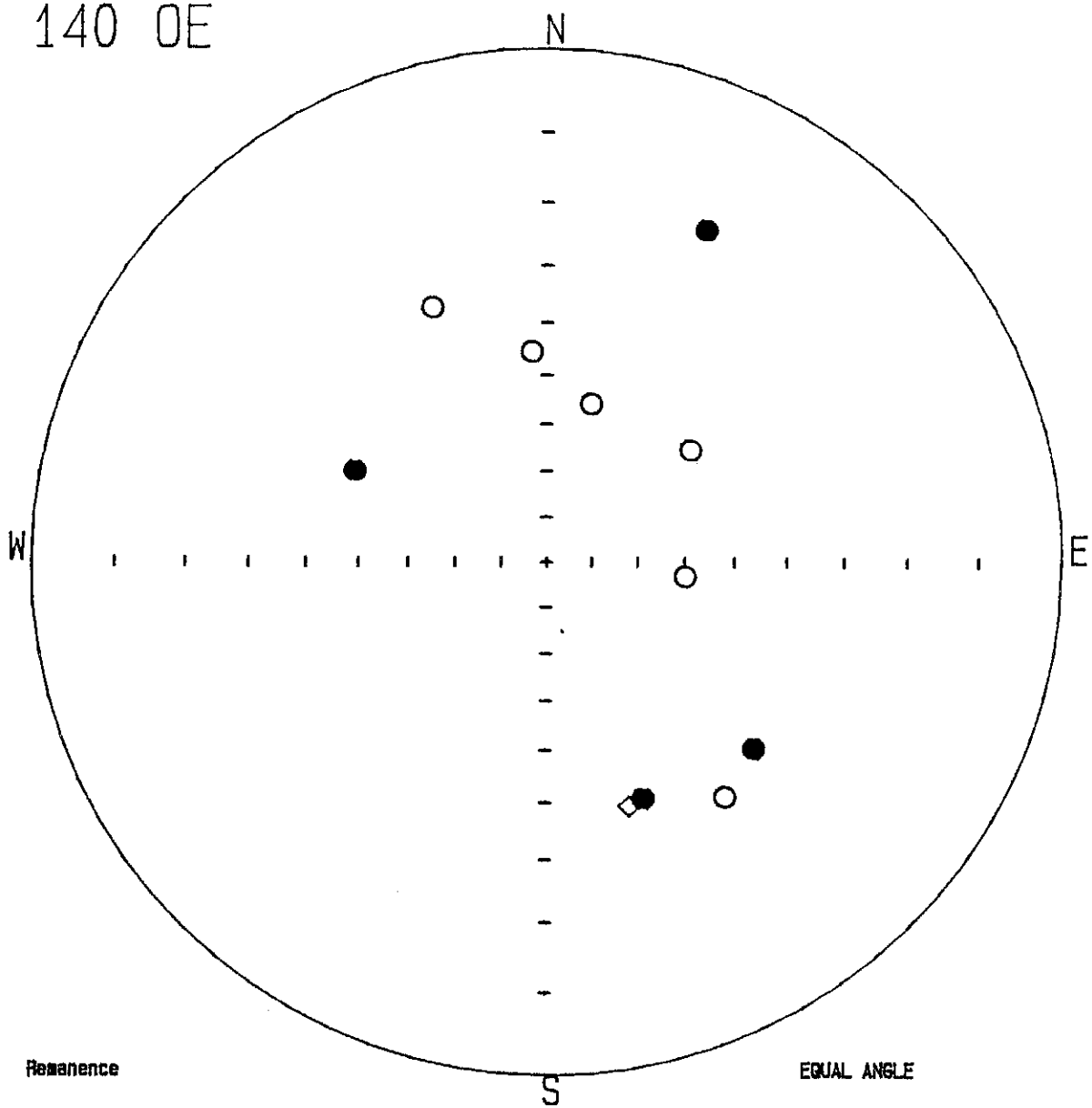

Fig.8. Thermal (550°C) cleaned remanence directions for Trough Tank bif.

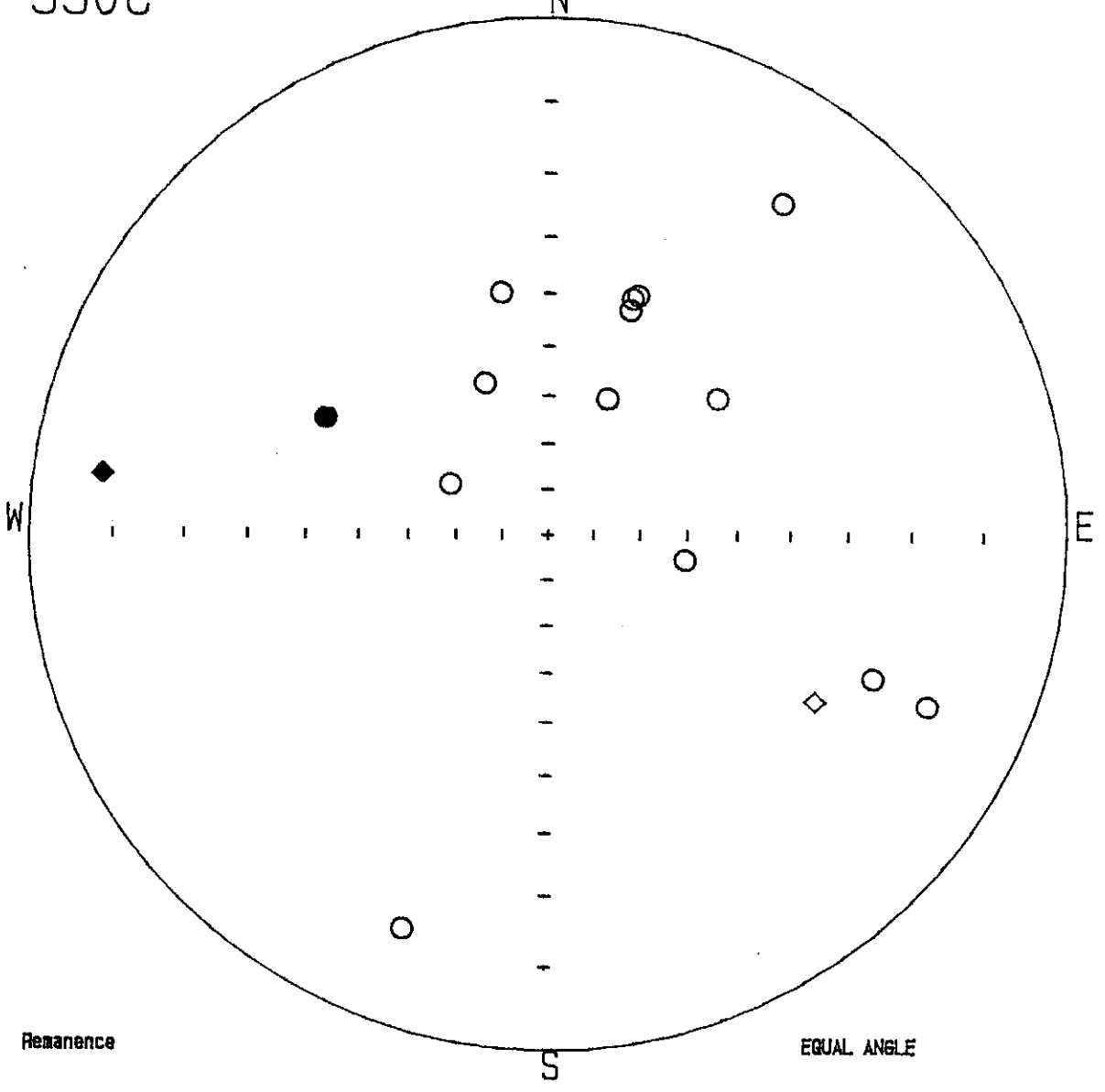
N
W
E
S
Remanence
EQUAL ANGLE

Fig.9. Explanation of orthogonal projections (Zijderveld plots) for display of demagnetisation data.

Magnetisation is a three dimensional vector quantity and difficulties arise when representing such on a flat surface. Two separate figures are required to display a three dimensional vector. Stereographic plots and an intensity decay curve have been very useful, especially when the direction of the cleaned magnetisation is of paramount importance. However, when an appreciation of the full vectorial nature of a magnetisation is required, orthogonal projections (Zijderveld, 1967) provide an ideal method of combining both the magnitude and directional information. This greatly assists the recognition and identification of multi-component magnetisations.

(a) This illustration portrays the magnetisation decay during eight demagnetisation steps, from an oblique perspective (southeast-up octant). $\tilde{J}_1 - \tilde{J}_2$ represents the vector difference between the first and second demagnetisation step, i.e. the magnetisation removed during the second step.

(b) By simply plotting the vector end-points the diagram is greatly clarified and a soft $(\tilde{J}_s)$ and hard $(\tilde{J}_h)$ magnetisation are evident, yet a unique identification of the direction or intensity of either is not possible from this single figure.

(c) Linear combination of magnetisations yields a resultant NRM $(\tilde{J}_o)$.

(d) By projecting vector end-points onto the horizontal plane and a vertical plane allows the composition of the magnetisation to be visualised.

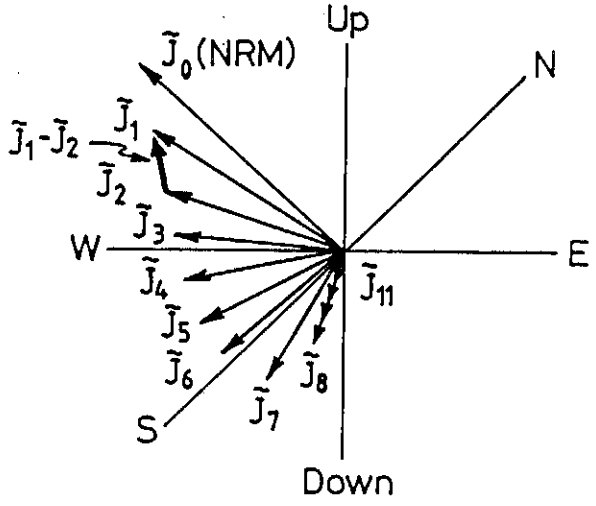

(c) Decomposition of two-component NRM

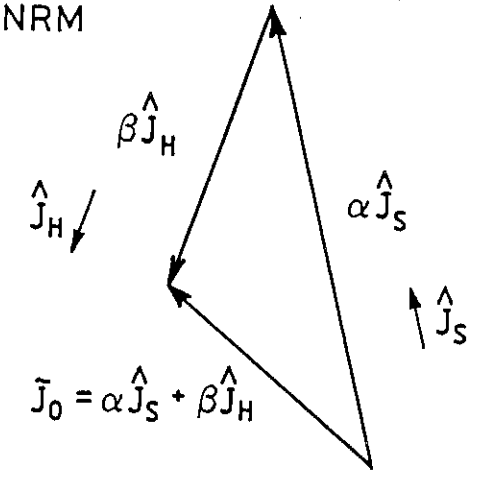

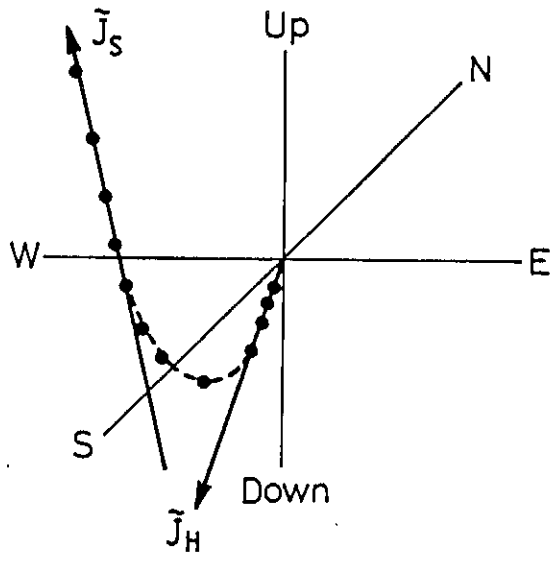

(d) Orthogonal projections

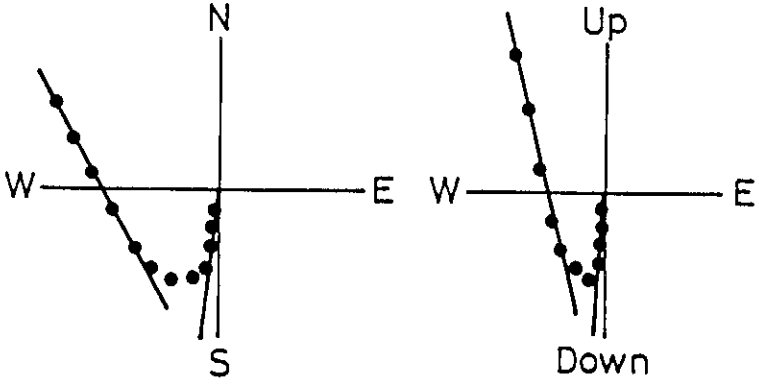

Fig.10. Representative Zijderveld plots for AF and thermal demagnetisation of specimens from Starra.

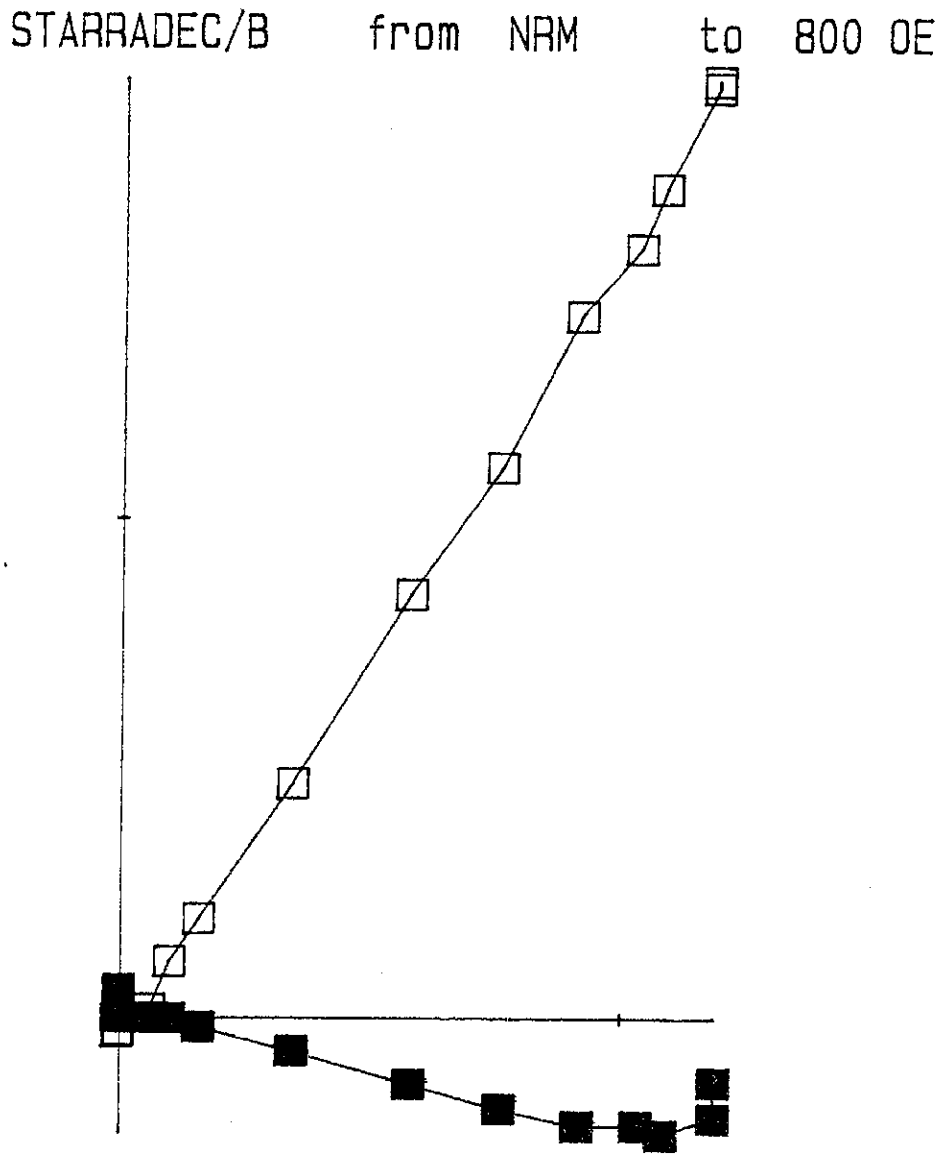
STARRADEC/B from NRM to 800 0E
down east
tick value is 1 * 10e3

STARRADEC/C from NRM to 615C

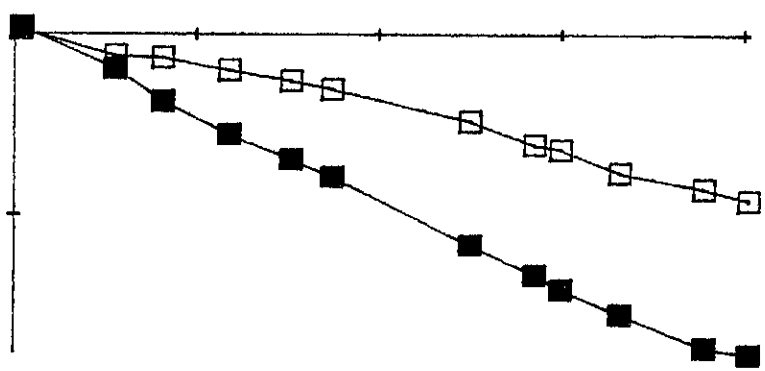

down east

tick value is 1 * 10e3

STARRA203B from NRM to 200 0E

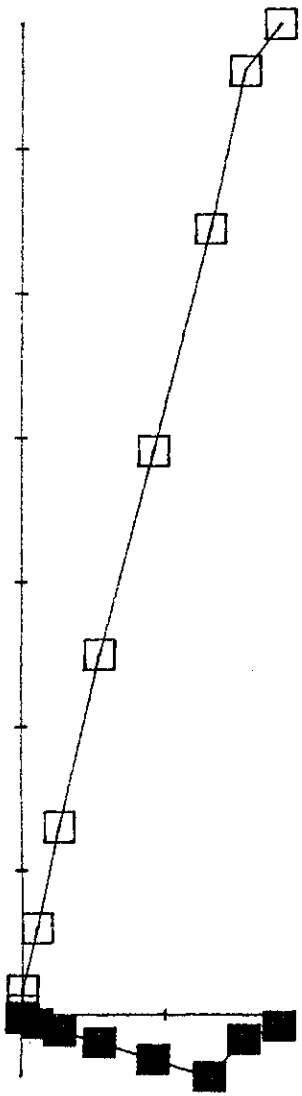

down south

tick value is 1 * 10e4

STARRA206B from NRM to 300 0E

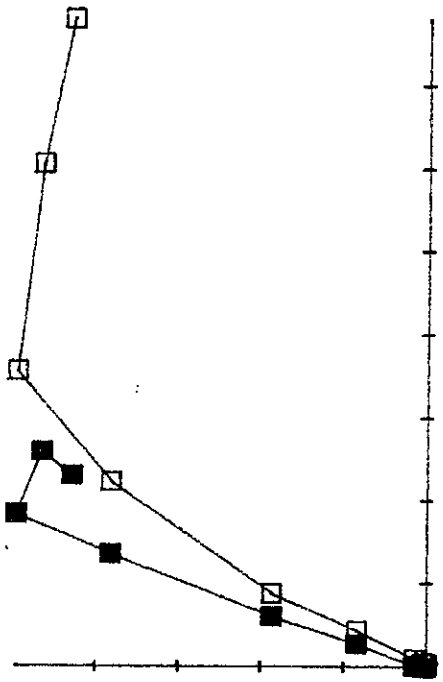

down east

tick value is 1 * 10e4

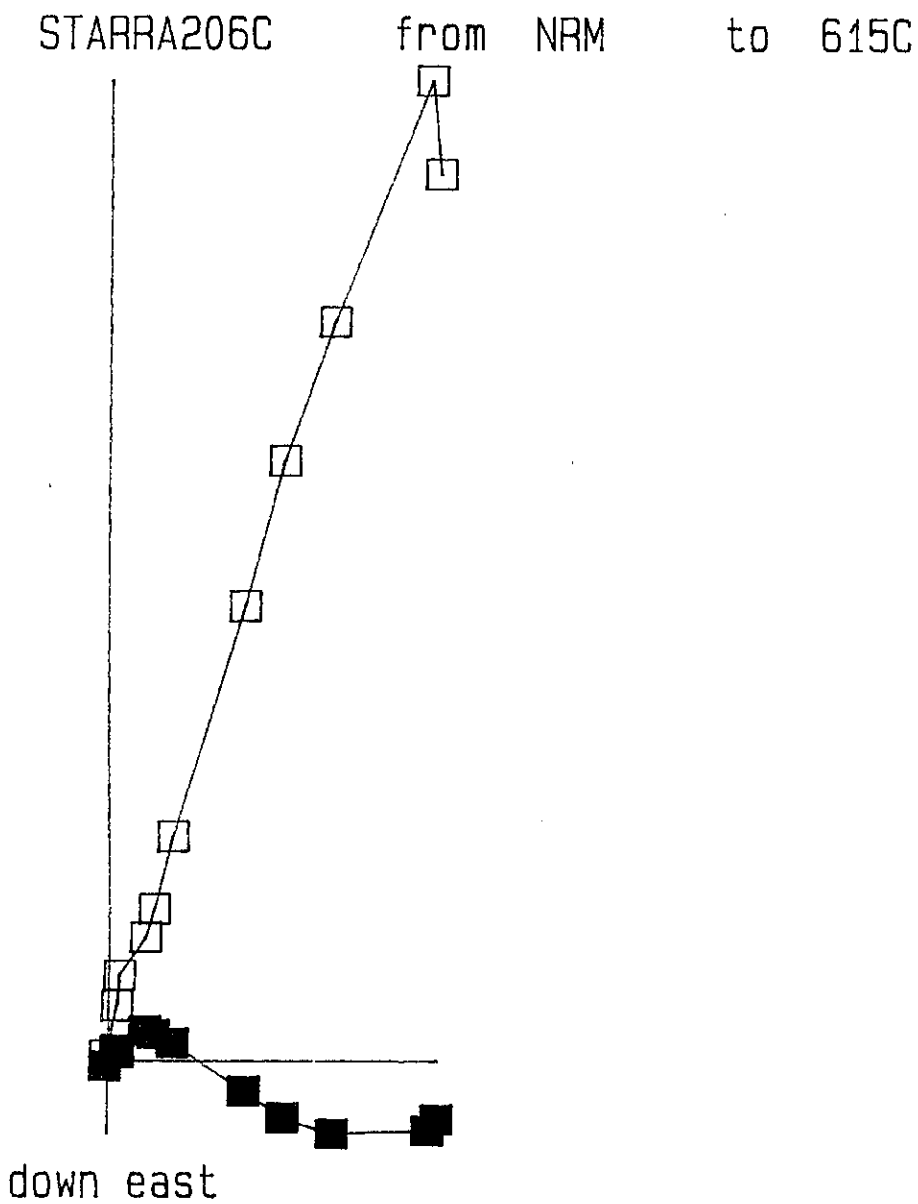
STARRA206C from NRM to 615C
down east
tick value is 1 * 10e5

tick value is 1 * 10e5

STARRA209A from VRM to 800 OE

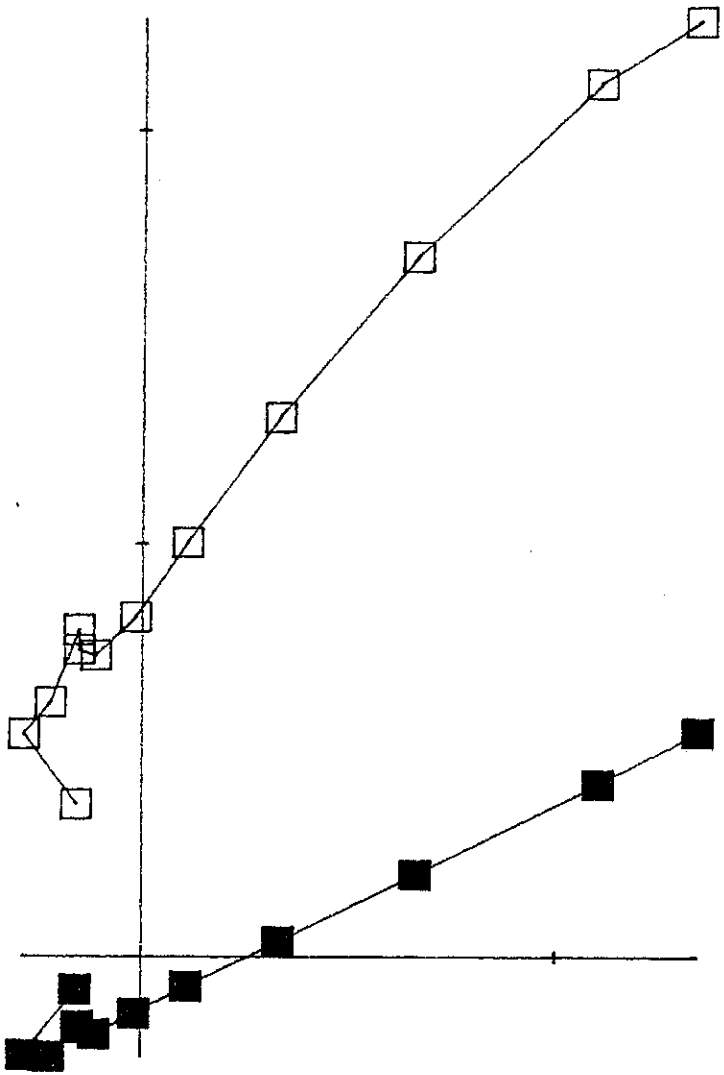

down south

tick value is 1 * 10e4

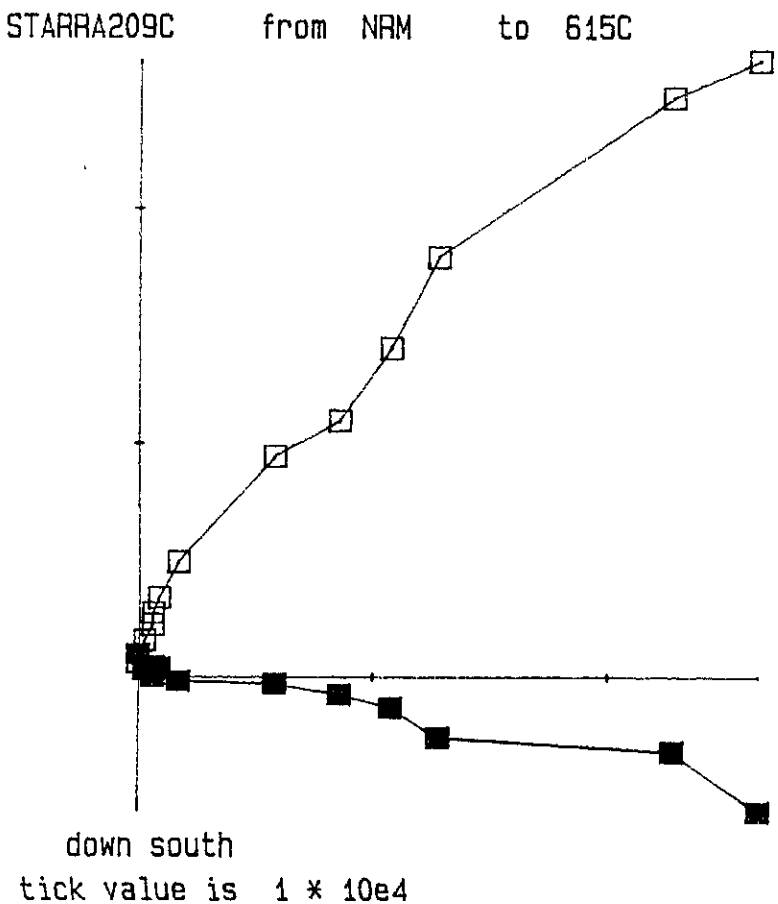
STARRA209C from NRM to 615C
down south
tick value is 1 * 10e4

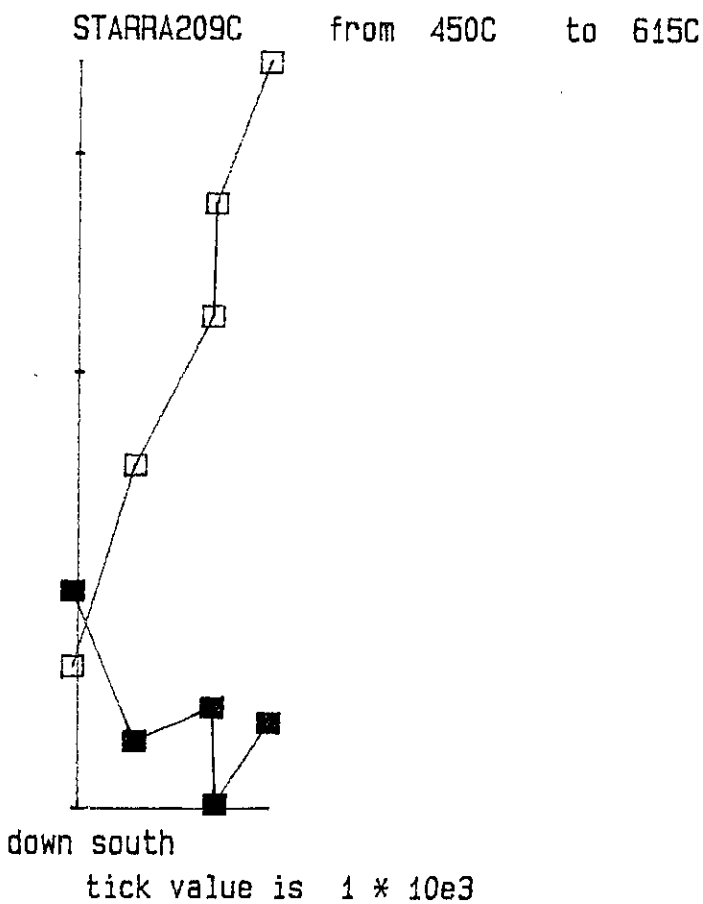
STARRA209C from 450C to 615C
down south
tick value is 1 * 10e3

STARRA284B from NRM to 200 OE

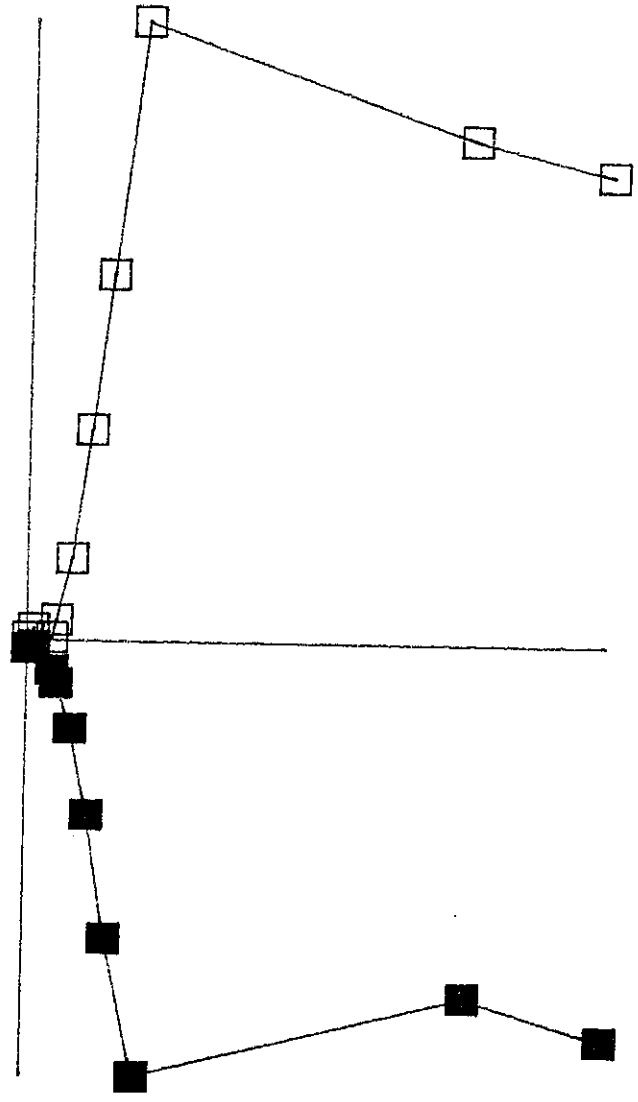

down south

tick value is 1 * 10e4

STARRA324A from NRM to 615C

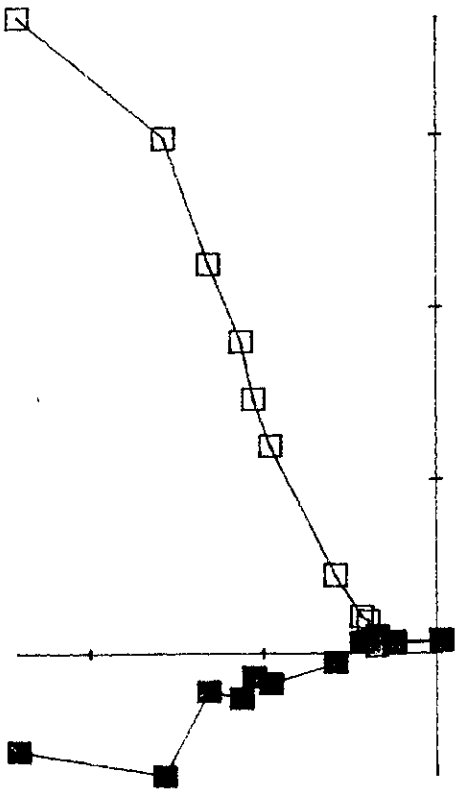

down east

tick value is 1 * 10e4

RRA324B from NRM to 200 0E

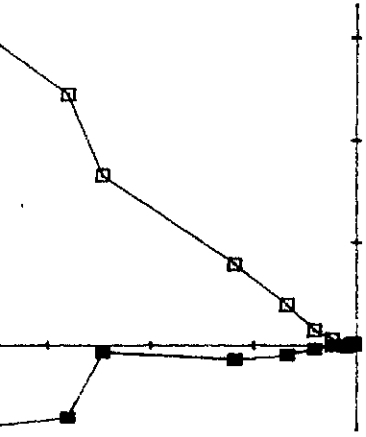

down east

ck value is 1 * 10e4

STARRA324B from 30 0E to 200 0E

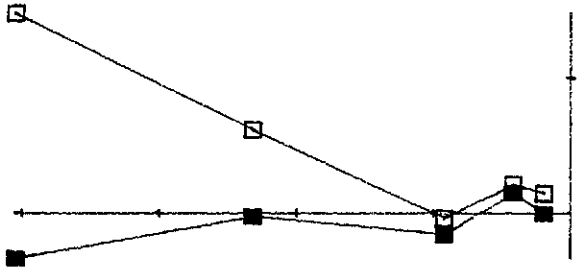

down east

tick value is 1 * 10e3

STARRA344A from NRM to 615C

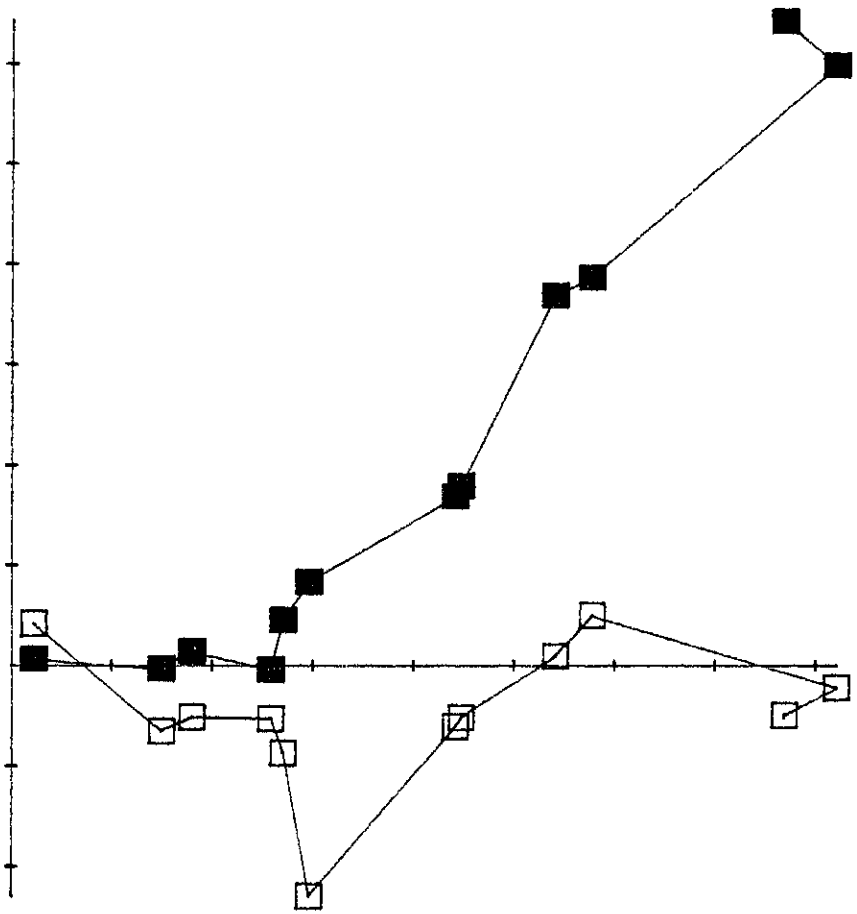

down south

tick value is 1 * 10e3

STARRA344B from VRM to 200 0E

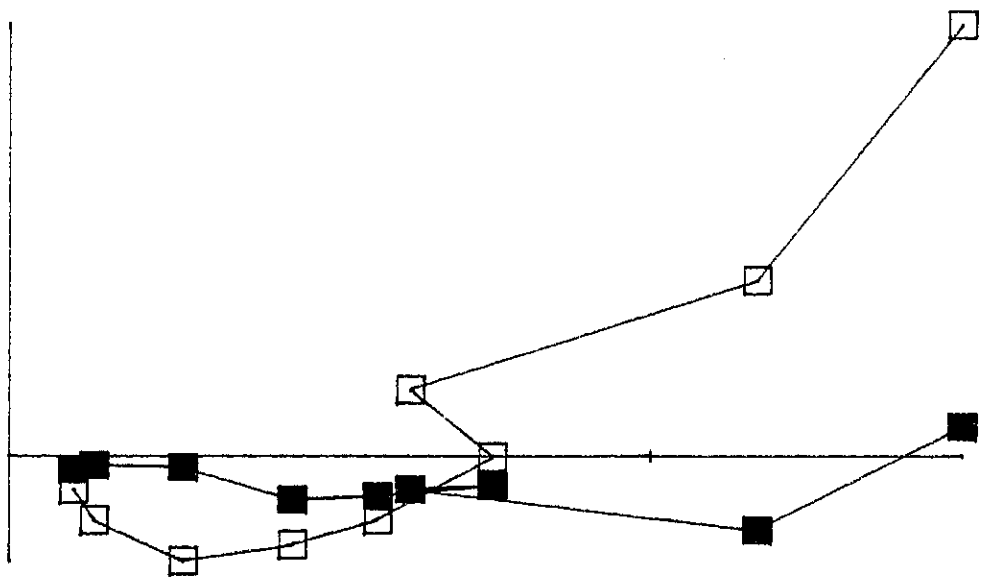

down south

tick value is 1 * 10e4

Fig.11. Representative Zijderveld plots for AF and thermal demagnetisation of Trough Tank specimens.

TTNQ3 61B from 200C to 615C

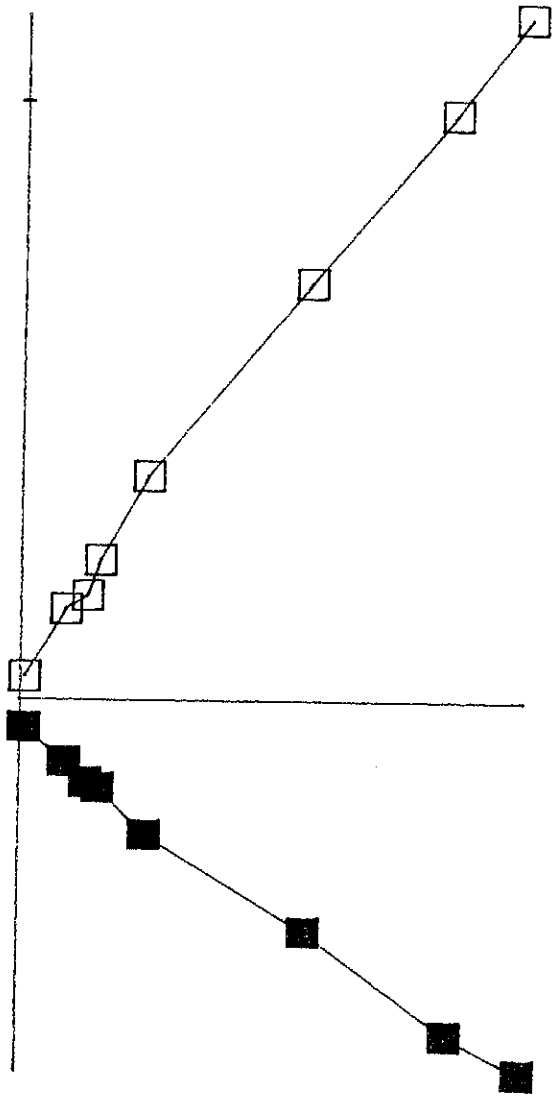

down east

tick value is 1 * 10e4

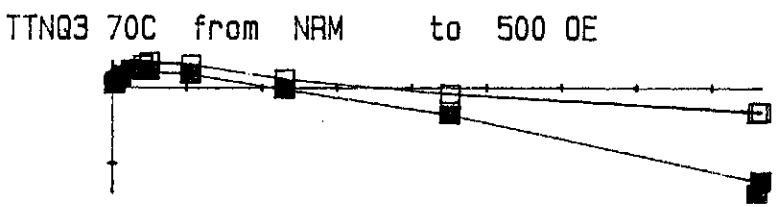
TTNQ3 70C from NRM to 500 0E
down east
tick value is 1 * 10e4

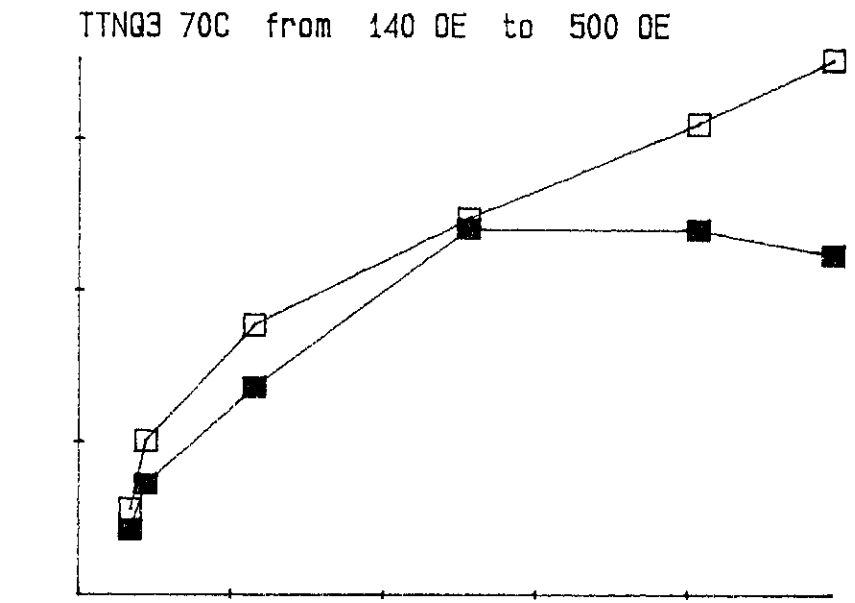
TTNQ3 70C from 140 0E to 500 0E
down east
tick value is 1 * 10e3

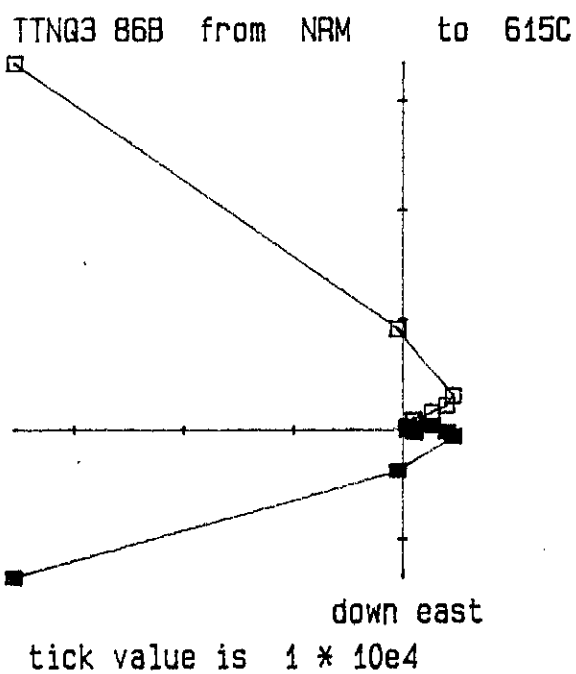
TTNQ3 86B from NRM to 615C
down east
tick value is 1 * 10e4

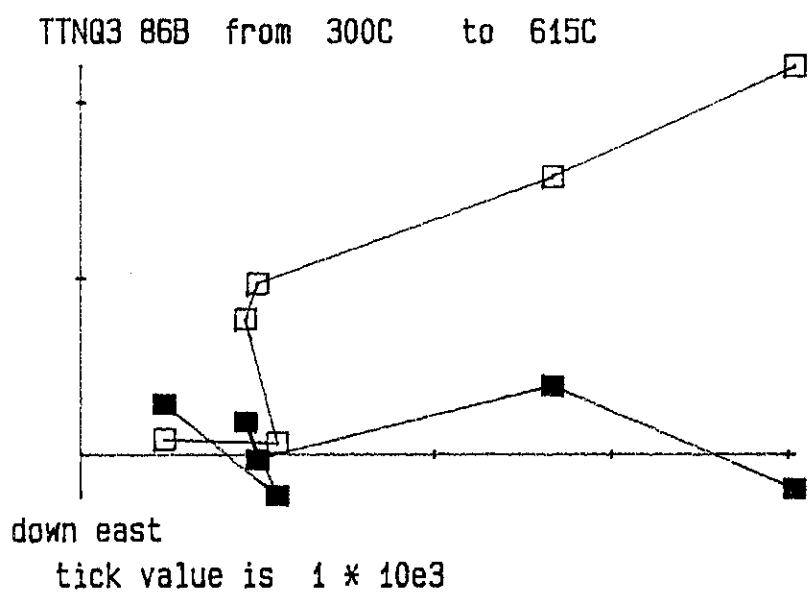
TTNQ3 86B from 300C to 615C
down east
tick value is 1 * 10e3

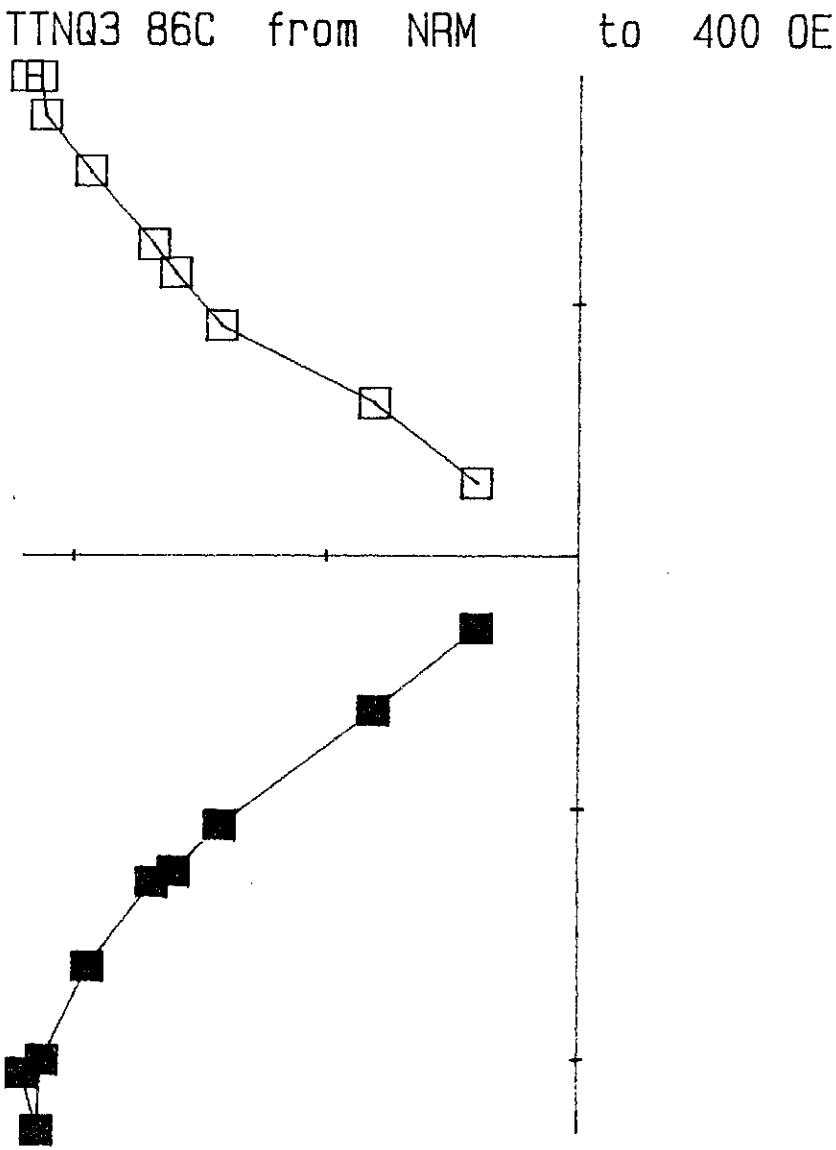
TTNQ3 86C from NRM to 400 0E
down east
tick value is 1 * 10e4

TTNQ3 114C from NRM to 615C

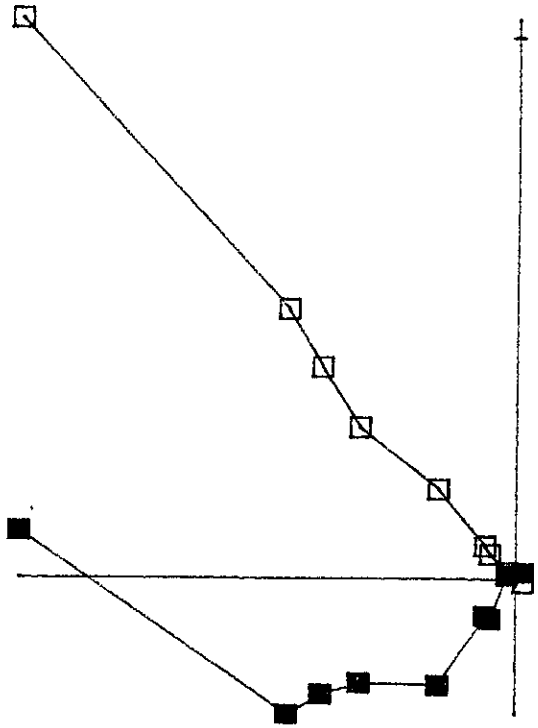

down east

tick value is 1 * 10e4

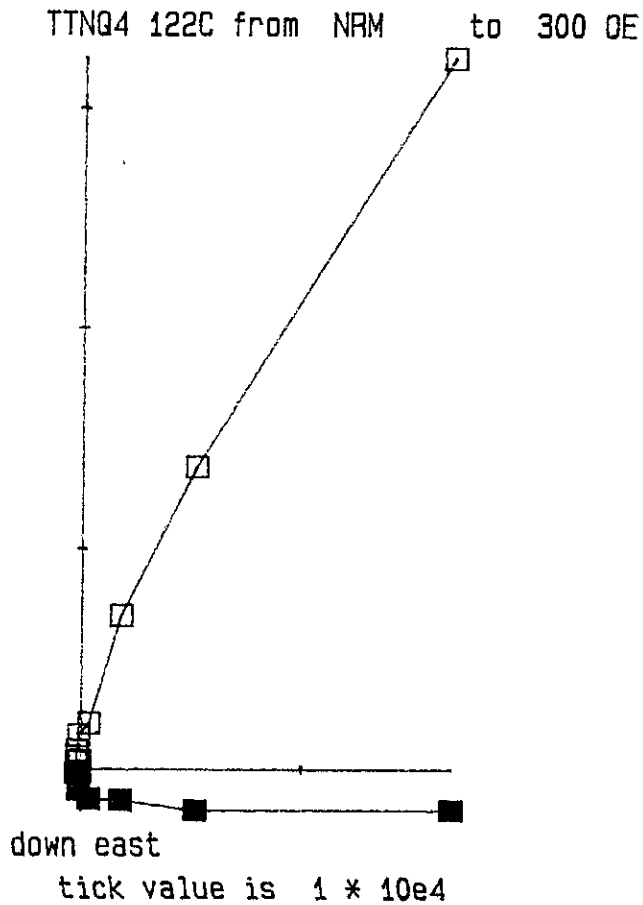
TTNQ4 122C from NRM to 300 0E
down east
tick value is 1 * 10e4

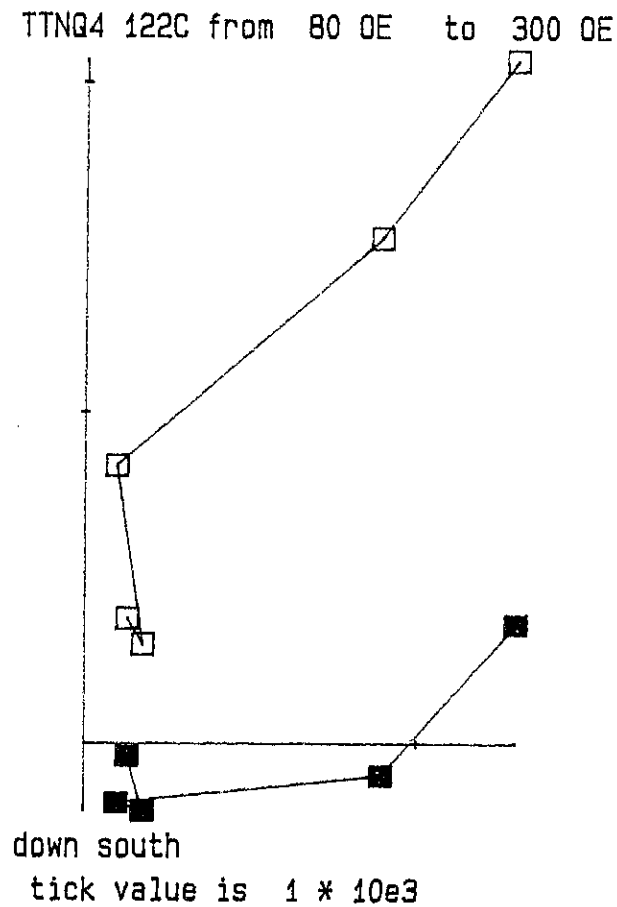
TTNQ4 122C from 80 0E to 300 0E
down south
tick value is 1 * 10e3

TTNQ4 132B from NRM to 100 mT

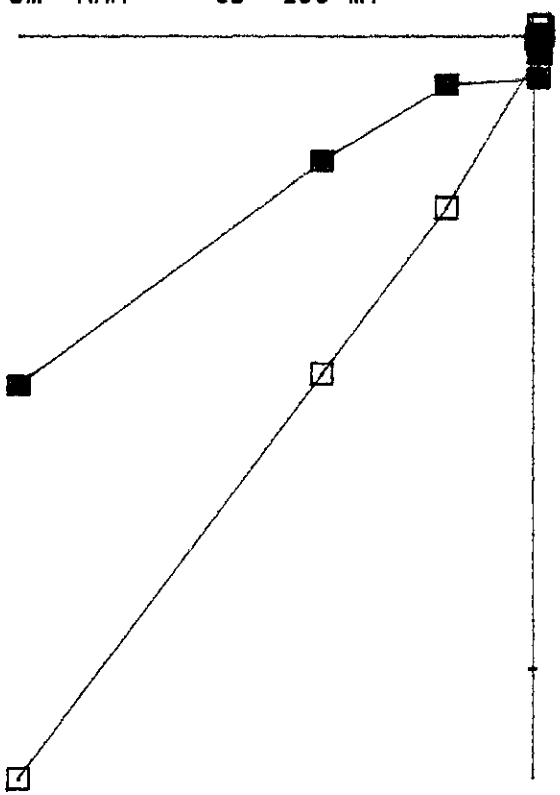

tick value is 1 * 10e4

TTNQ4 132B from 80 OE to 100 mT

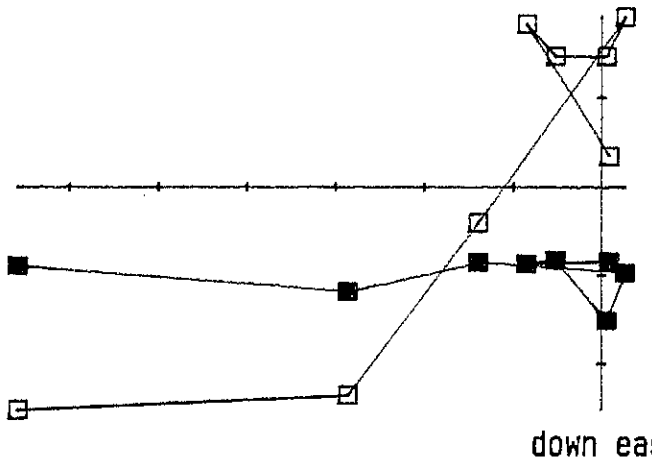

tick value is 1 * 10e2

TTNQ4 132B from NRM to 100 mT

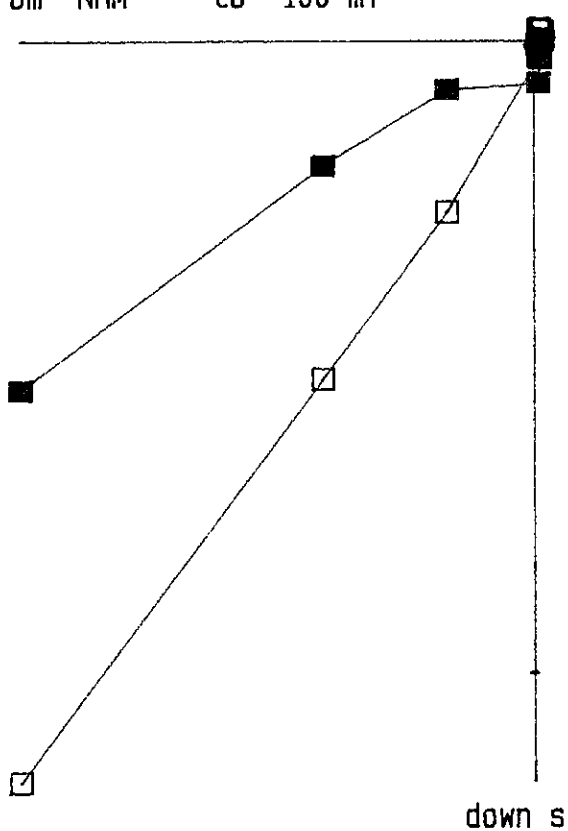

down south

tick value is 1 * 10e4

TTNQ4 132B from 80 OE to 100 mT

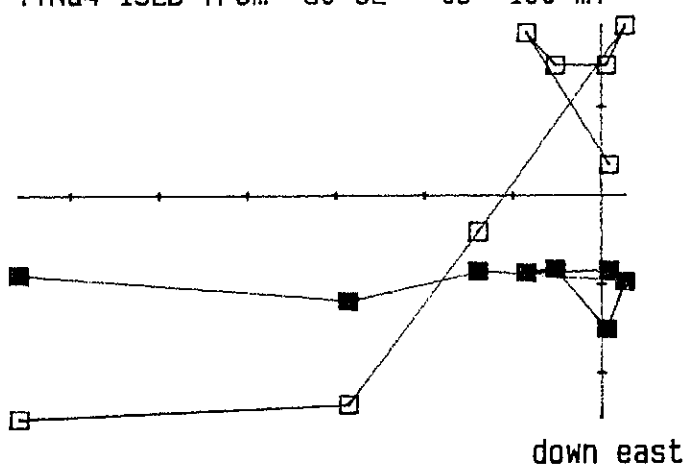

down east

tick value is 1 * 10e2

tick value is 1 * 10e4

TTNQ6 114C from NRM to 200 OE

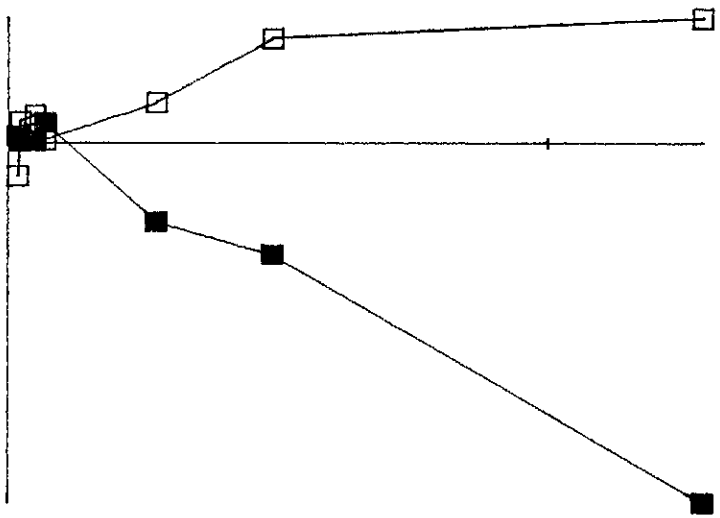

down east

tick value is 1 * 10e4

Fig.12. Orientation of principal susceptibility axes of specimens from the Starra decline sample.

STARRAFC.sus
DEC

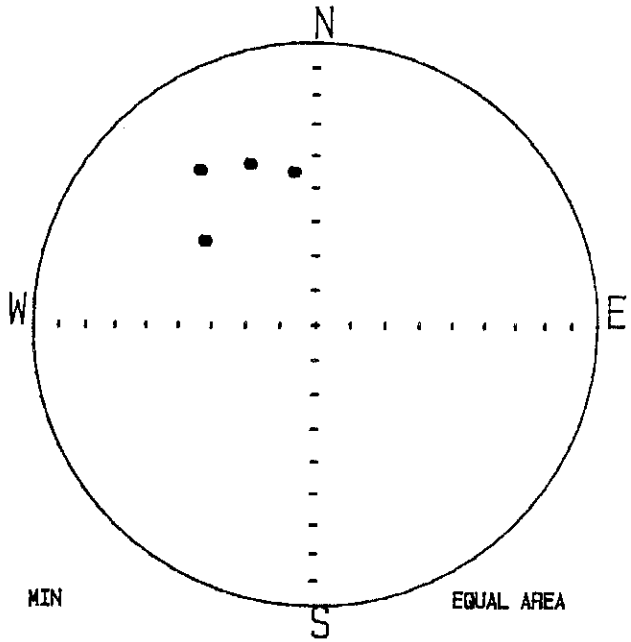

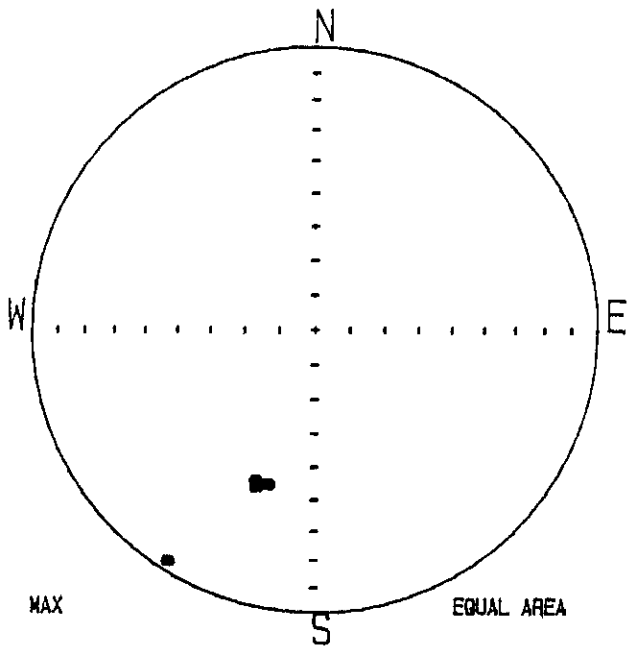

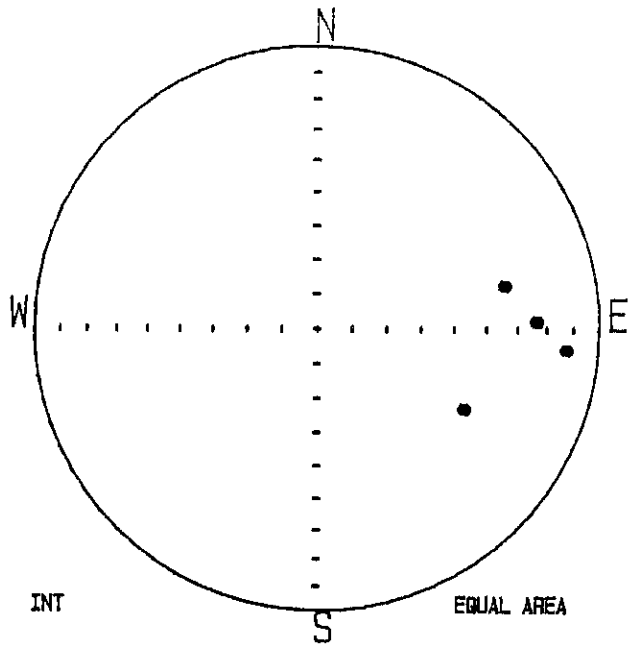

Fig.13. Orientation of principal susceptibility axes of quartz-magnetite specimens from Starra.

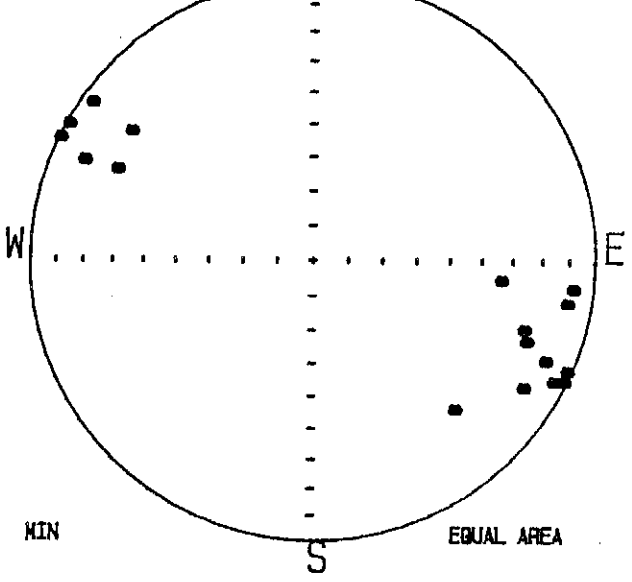
W
E
S
MIN
EQUAL AREA

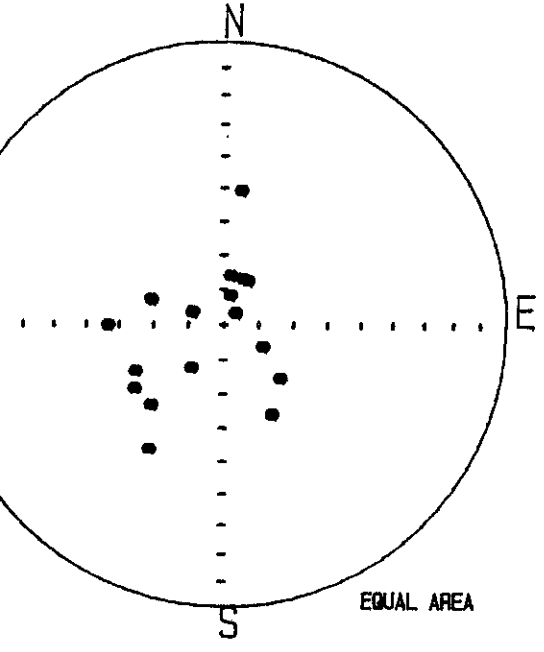
N
E
S
EQUAL AREA

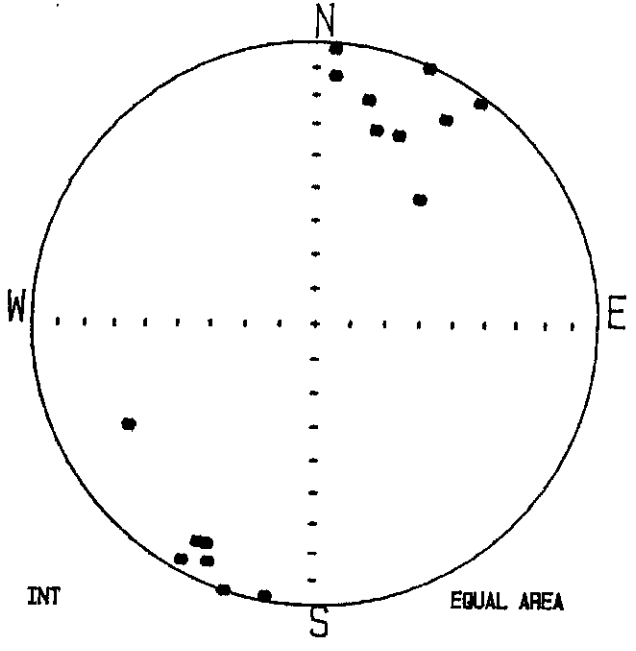
N
W
E
S
INT
EQUAL AREA

Fig.14. Orientation of principal susceptibility axes of Trough Tank specimens.

ttankfc.sus

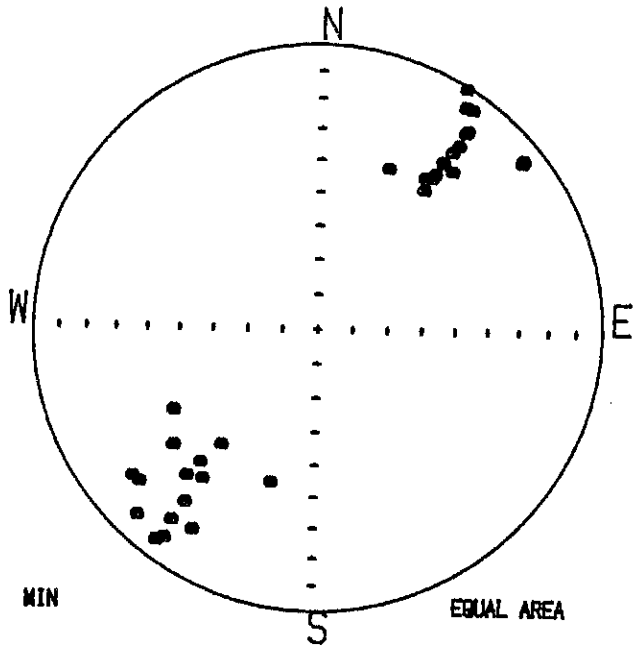

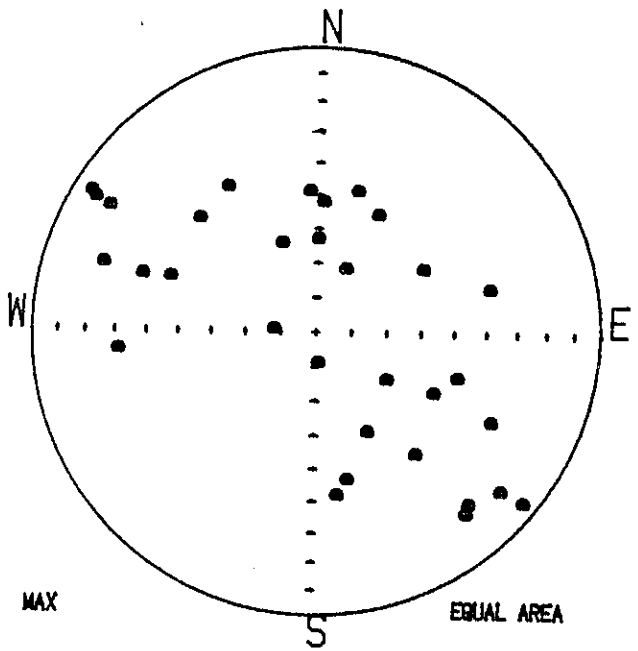

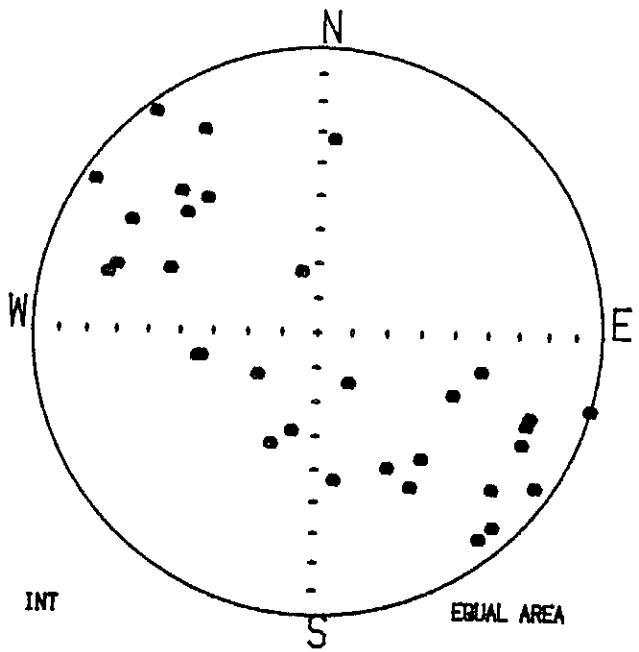

Fig.15. Relationships between component anomalies, the measured scalar intensity anomaly and the conventionally calculated total field anomaly.

SCHEMATIC RELATIONSHIP BETWEEN MEASURED, TRUE AND CALCULATED TOTAL MAGNETIC INTENSITY ANOMALIES

Southern hemisphere fields depicted with negative inclination

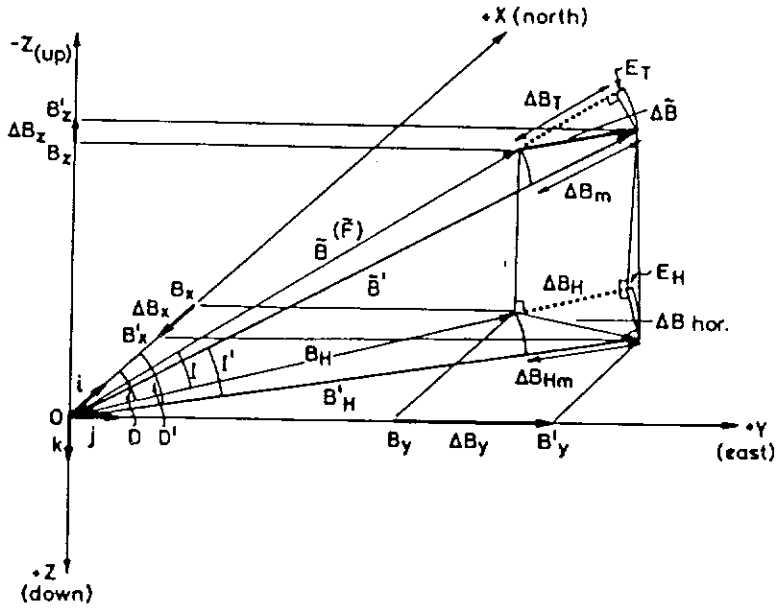

$\Delta B_T = \Delta B_H \cos I + \Delta B_z \sin I$ (computed total field anomaly)

$\Delta B_m = |\tilde{B}'| - |\tilde{B}|$ (measured total field anomaly)

$\Delta E_T = \Delta B_m - \Delta B_T = (|\Delta\tilde{B}|^2 - \Delta B_m^2)/2|\tilde{B}|$, $|\Delta\tilde{B}| \neq \Delta B_T \neq \Delta B_m$

D (= D) is the angle between the +X axis and the horizontal projection of the field vector (ℓ,m,n)

$\tilde{i}$, $\tilde{j}$, $\tilde{k}$ unit vectors parallel to X, Y, Z axes respectively

ℓ, m, n direction cosines. For $\tilde{B}(F)$: $\ell = B_x/|\tilde{B}|$, $m = B_y/|\tilde{B}|$, $n = B_z/|\tilde{B}|$

$\ell\tilde{i} + m\tilde{j} + n\tilde{k}$ unit vector in direction (ℓ,m,n)

$\Delta\tilde{B}$ local magnetic anomaly vector, perturbing $\tilde{B}$

$\tilde{B}(\tilde{F})$ regional or "normal" magnetic field vector of Earth (constant over limited region)

$\tilde{B}'$ resultant (local) field = $\tilde{B} + \Delta\tilde{B}$; with declination D', inclination I'

ΔB_T component of $\Delta\tilde{B}$ along normal field $\tilde{B}$. This is the theoretical computed anomaly. Usually $\Delta B_T \tilde{<} \Delta B_m$

ΔB_m measured residual total field anomaly (scalar measurement of variation in magnitude of resultant field)

E_T departure of computed anomaly (ΔB_T) from measured anomaly (ΔB_m). Usually small

ΔB_{hor} horizontal projection of $\Delta\tilde{B}$ = true horizontal component of anomalous field

B_H component of $\tilde{B}(\tilde{F})$ along regional magnetic meridian

B_H' component of $\tilde{B}'$ along local anomalous magnetic meridian

ΔB_H computed horizontal field anomaly = component of $\Delta\tilde{B}$ along regional magnetic meridian

ΔB_{H_m} measured horizontal field anomaly $\Delta B_{H_m} = B_H' - B_H \neq \Delta B_{hor} \neq \Delta B_H$

$E_H = (\Delta B_H^2 - \Delta B_{H_m}^2)/2B_H = B_H'\{1-\cos(D'-D)\}$. Departure of computed from measured horizontal anomaly

ΔB_x true horizontal anomaly component along X axis = $B_x' - B_x$

ΔB_y true horizontal anomaly component along Y axis = $B_y' - B_y$

$\Delta B_{hor} = (\Delta B_x^2 + \Delta B_y^2)^{\frac{1}{2}}$

ΔB_z true vertical intensity anomaly, measured anomaly = vertical component.

Fig.17. Non-uniqueness of interpreted dip.

NON—UNIQUENESS

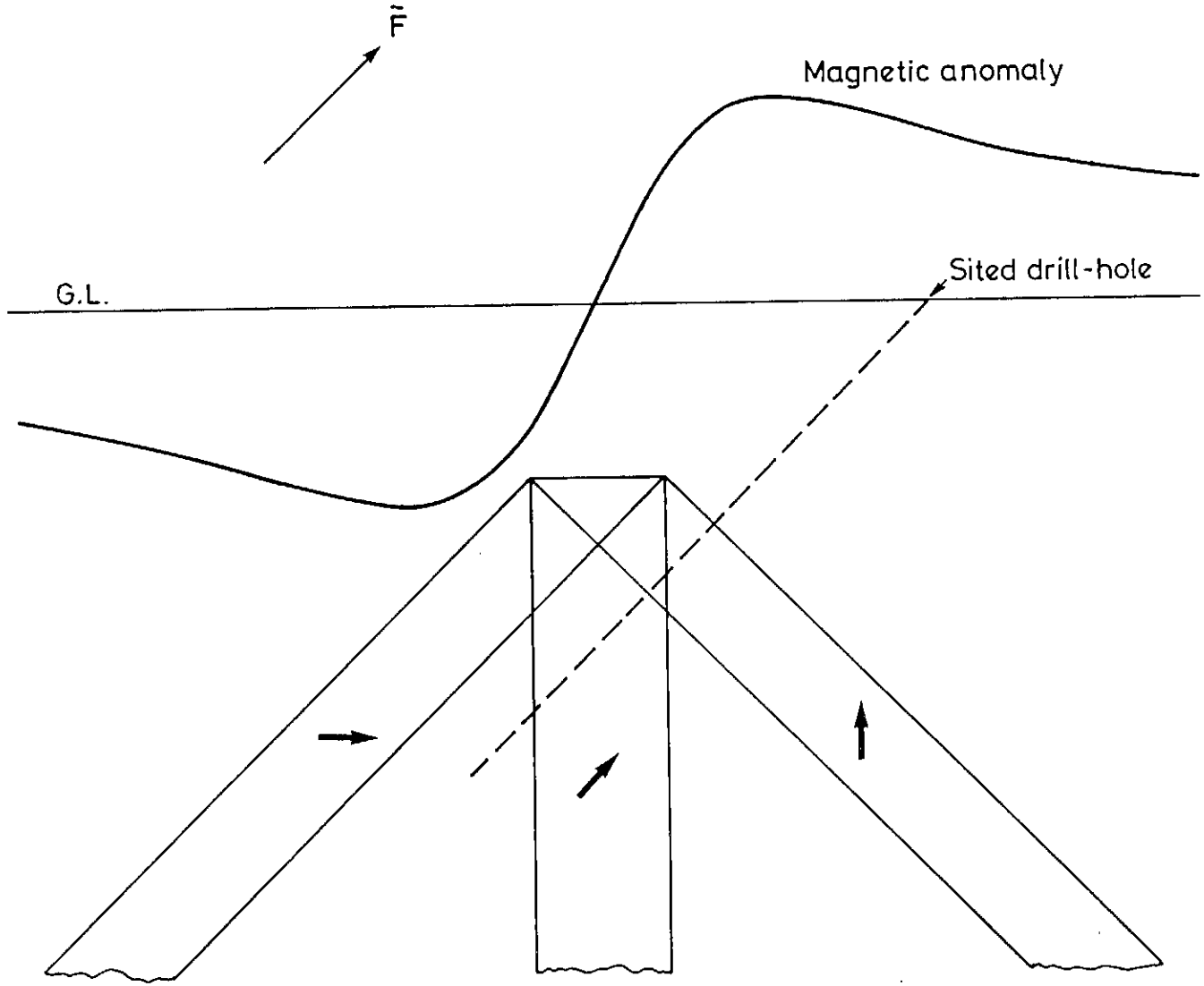

Fig.18. Anomaly due to the anisotropic component of induced magnetisation.

ANISOTROPIC DIPPING SHEETS (A=∞, Q=0)

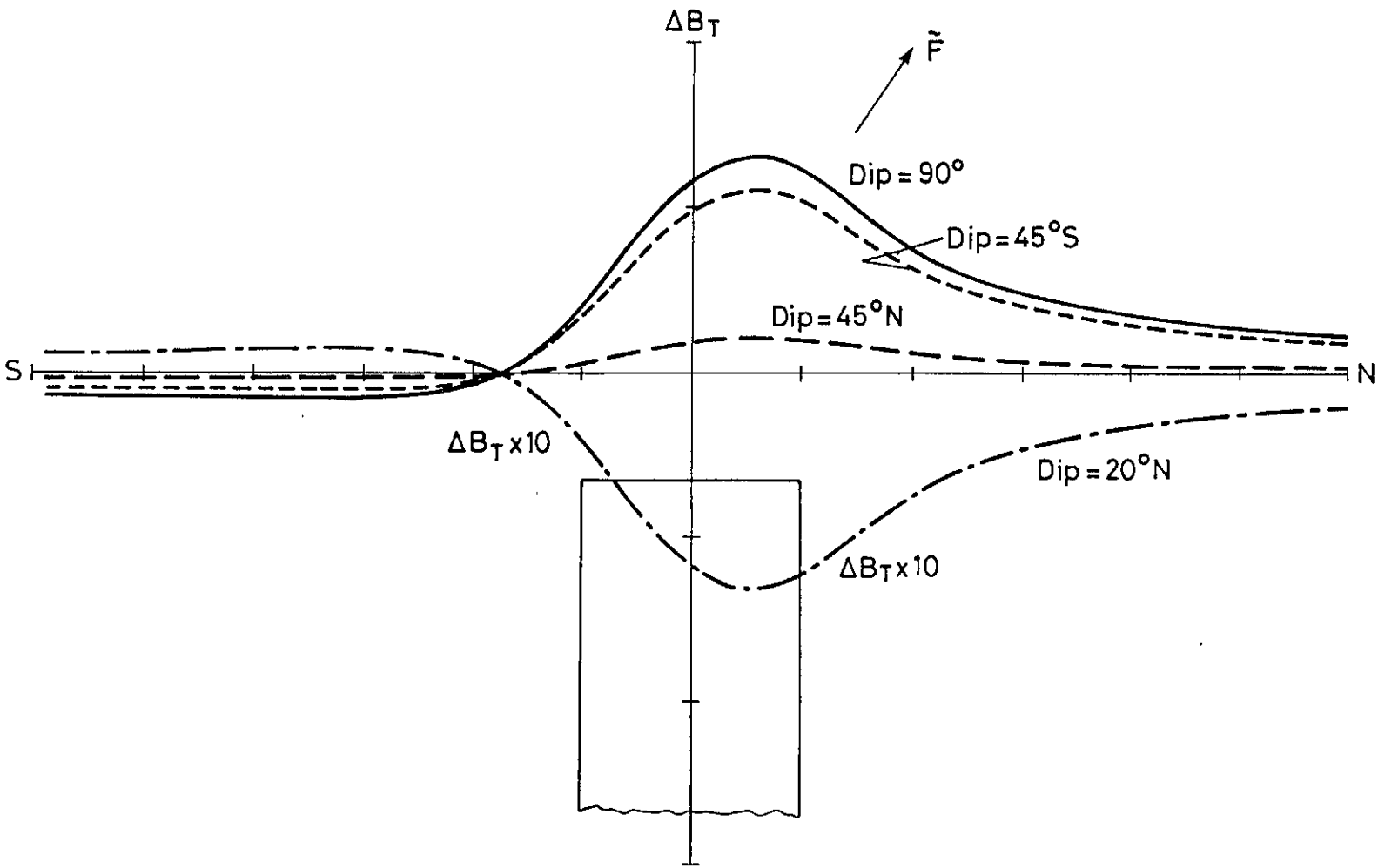

Fig.20. Anomalous apparent dip of Trough Tank bif due to self-demagnetisation.

FIG. 20 ANOMALOUS APPARENT DIP OF TROUGH TANK BIF

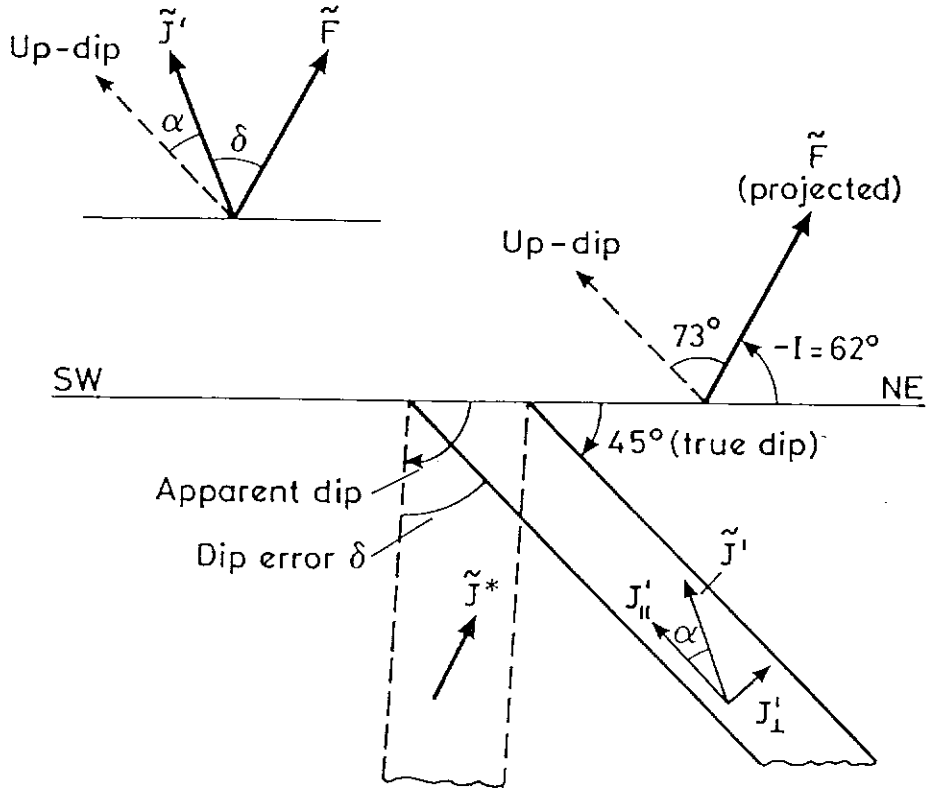

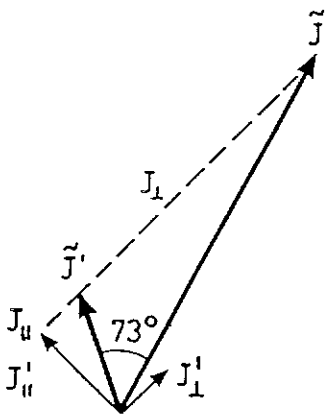

Without self-demagnetisation:

$J_{II} = kF \cos 73°$

$J_{\perp} = kF \sin 73°$

With self-demagnetisation:

$J'_{II} = J_{II} \quad (N_{II} = 0)$

$J'_{\perp} = \dfrac{J_{\perp}}{1 + 4\pi k} \quad (N_{\perp} = 4)$

$\therefore \tan \alpha = \dfrac{J'_{\perp}}{J'_{II}} = \dfrac{\tan 73°}{1 + 4\pi k}$

Fig.21. Dip dependence of B_m and B_T anomalies at Trough Tank.

FIG. 21 DIP DEPENDENCE OF ΔB_m AND ΔB_T ANOMALIES

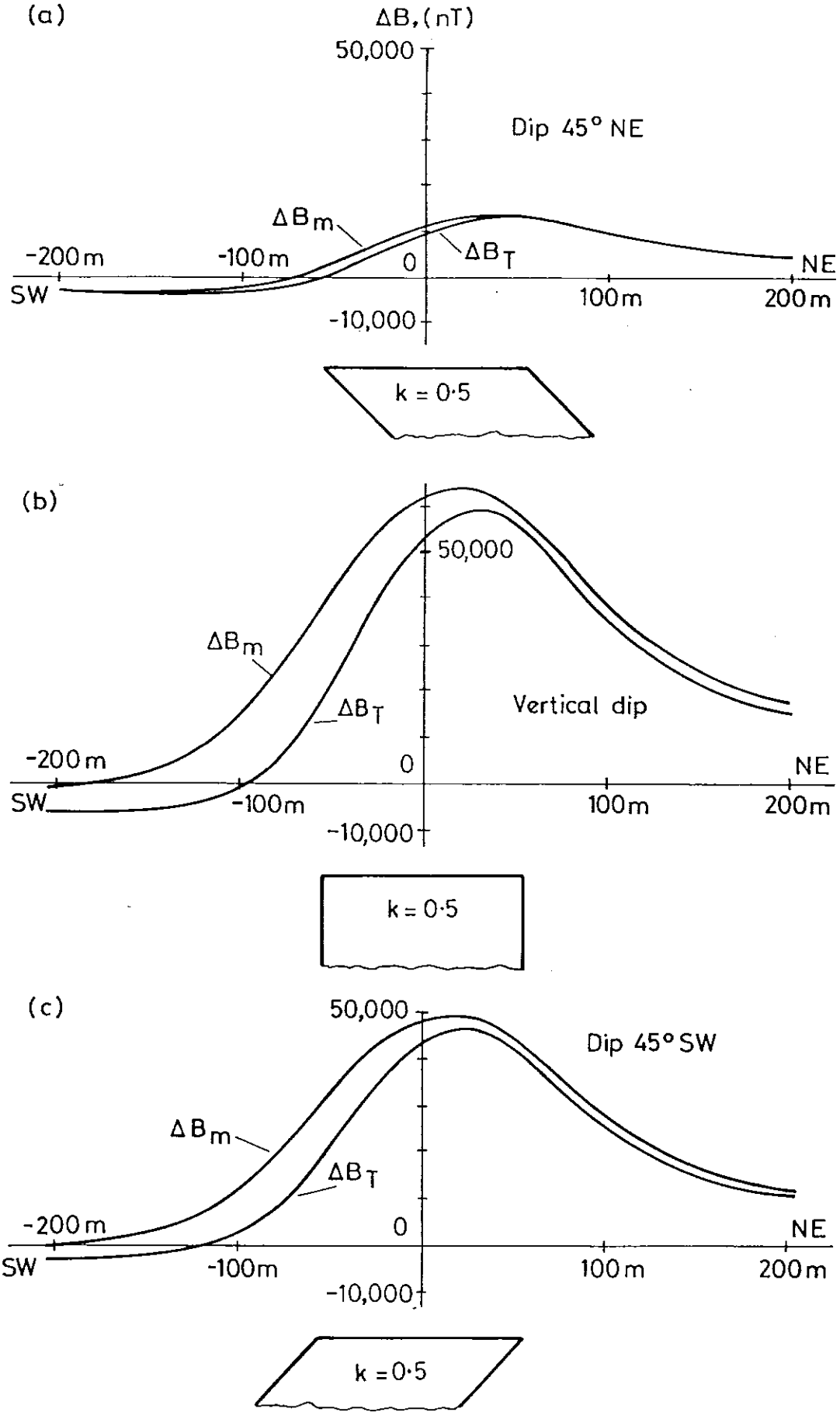

Fig.22. Effects of self-demagnetisation and intrinsic anisotropy on anomaly shape at Trough Tank.

FIG. 22 EFFECTS OF SELF—DEMAGNETISATION AND ANISOTROPY ON ANOMALY SHAPE